result of minute inflammation. However, whether such pretransplant status can cause an increased incidence of chronic GVHD remains unclear and requires clarification in future studies.

In contrast to the positive association between elevated CRP levels and the development of chronic GVHD, we observed an inverse association trend between high ferritin levels and the development of chronic GVHD, as previously reported by others, though it was not statistically significant ($P = 0.099$), [6, 7]. In a subgroup analysis, we observed a significant association between the high ferritin levels and the development of chronic GVHD in patients with myeloid malignancies, but not in those with lymphoid malignancies. The reason why this association was observed only in those with myeloid malignancies is uncertain. Further well-designed studies are needed to confirm this result.

Ferritin, a heteropolymer comprising 24 H- and L-type subunits, has been suggested to play a role as an immune regulator [27]. Several lines of evidence have demonstrated that ferritin can suppress the proliferation of T cells in response to mitogens, impair the maturation of B cells, and inhibit the proliferation of myeloid cells [28–30]. H-ferritin has been suggested to induce the production of interleukin 10 from regulatory T cells and suppress immune responses [31, 32]. In the light of these findings, among the patients with myeloid malignancies, the decreased incidence of chronic GVHD and significantly higher relapse rate, as determined by the multivariate analysis, in the high-ferritin group (Table 3) may be related to the suppressive effect of ferritin on adaptive immune responses. Given that ferritin levels are increased not only by iron overload but also by other factors such as inflammation, the objective measurement of liver iron content using magnetic resonance imaging [33] will be helpful in providing a more accurate analysis of the association between pretransplant iron overload and the incidence of chronic GVHD.

Several limitations of this study should be mentioned. First, the retrospective study design and heterogeneous background of the diseases and transplantation procedures might have biased the results. Second, posttransplant serum ferritin levels were not evaluated in this cohort owing to the lack of adequate information. We could obtain post-transplant (between day +50 and +99) serum ferritin data from only 28 cases among our cohort. Third, although we included CRP in the multivariate analysis, it was difficult to adjust for the effect of factors other than iron overload on ferritin levels. In a future study, measuring serum ferritin levels and liver iron content using magnetic resonance imaging before and after transplantation, and reanalyzing the effect of iron overload on the outcome may be worthwhile.

In conclusion, our results suggest that the pretransplant serum ferritin levels influenced the incidences of TRM and relapse rate after allogeneic HSCT and that, overall, an elevated pretransplant serum ferritin level is a strong adverse prognostic factor for survival. Furthermore, our results also suggest that a pretransplant serum CRP level may be a useful biomarker for predicting the risk of chronic GVHD.

Acknowledgments The authors would like to thank Rie Goi and Mika Kobayashi for their expert data management and secretarial assistance, and all the staff of our transplant team for their dedicated care of the patients and donors. This work was supported in part by a grant-in-aid for scientific research from the Ministry of Education, Culture, Sports, Science and Technology of Japan.

Conflict of interest The authors declare that they have no conflict of interest.

References

1. Majhail NS, Lazarus HM, Burns LJ. Iron overload in hematopoietic cell transplantation. Bone Marrow Transpl. 2008;41(12):997–1003.
2. Altes A, Remacha AF, Sureda A, Martino R, Briones J, Canals C, et al. Iron overload might increase transplant-related mortality in haematopoietic stem cell transplantation. Bone Marrow Transpl. 2002;29(12):987–9.
3. Armand P, Kim HT, Cutler CS, Ho VT, Koreth J, Alyea EP, et al. Prognostic impact of elevated pretransplantation serum ferritin in patients undergoing myeloablative stem cell transplantation. Blood. 2007;109(10):4586–8.
4. Pullarkat V, Blanchard S, Tegtmeier B, Dagis A, Patane K, Ito J, et al. Iron overload adversely affects outcome of allogeneic hematopoietic cell transplantation. Bone Marrow Transpl. 2008;42(12):799–805.
5. Kataoka K, Nannya Y, Hangaishi A, Imai Y, Chiba S, Takahashi T, et al. Influence of pretransplantation serum ferritin on nonrelapse mortality after myeloablative and nonmyeloablative allogeneic hematopoietic stem cell transplantation. Biol Blood Marrow Transpl. 2009;15(2):195–204.
6. Mahindra A, Bolwell B, Sobecks R, Rybicki L, Pohlman B, Dean R, et al. Elevated pretransplant ferritin is associated with a lower incidence of chronic graft-versus-host disease and inferior survival after myeloablative allogeneic haematopoietic stem cell transplantation. Br J Haematol. 2009;146(3):310–6.
7. Wahlin A, Lorenz F, Fredriksson M, Remberger M, Wahlin BE, Hagglund H. Hyperferritinemia is associated with low incidence of graft versus host disease, high relapse rate, and impaired survival in patients with blood disorders receiving allogeneic hematopoietic stem cell grafts. Med Oncol. 2011;28(2):552–8.
8. Lim ZY, Fiaccadori V, Gandhi S, Hayden J, Kenyon M, Ireland R, et al. Impact of pre-transplant serum ferritin on outcomes of patients with myelodysplastic syndromes or secondary acute myeloid leukaemia receiving reduced intensity conditioning allogeneic haematopoietic stem cell transplantation. Leuk Res. 2010;34(6):723–7.
9. Black S, Kushner I, Samols D. C-reactive Protein. J Biol Chem. 2004;279(47):48487–90.
10. Gabay C, Kushner I. Acute-phase proteins and other systemic responses to inflammation. N Engl J Med. 1999;340(6):448–54.

11. Artz AS, Wickrema A, Dinner S, Godley LA, Kocherginsky M, Odenike O, et al. Pretreatment C-reactive protein is a predictor for outcomes after reduced-intensity allogeneic hematopoietic cell transplantation. Biol Blood Marrow Transpl. 2008;14(11): 1209–16.
12. Fuji S, Kim SW, Fukuda T, Mori S, Yamasaki S, Morita-Hoshi Y, et al. Preengraftment serum C-reactive protein (CRP) value may predict acute graft-versus-host disease and nonrelapse mortality after allogeneic hematopoietic stem cell transplantation. Biol Blood Marrow Transpl. 2008;14(5):510–7.
13. Remberger M, Mattsson J. C-reactive protein levels before reduced-intensity conditioning predict outcome after allogeneic stem cell transplantation. Int J Hematol. 2010;92(1):161–7.
14. Kanda J, Mizumoto C, Ichinohe T, Kawabata H, Saito T, Yamashita K, et al. Pretransplant serum ferritin and C-reactive protein as predictive factors for early bacterial infection after allogeneic hematopoietic cell transplantation. Bone Marrow Transpl. 2011;46(2):208–16.
15. Giralt S, Ballen K, Rizzo D, Bacigalupo A, Horowitz M, Pasquini M, et al. Reduced-intensity conditioning regimen workshop: defining the dose spectrum. Report of a workshop convened by the center for international blood and marrow transplant research. Biol Blood Marrow Transpl. 2009;15(3):367–9.
16. Przepiorka D, Weisdorf D, Martin P, Klingemann HG, Beatty P, Hows J, et al. 1994 Consensus conference on acute GVHD grading. Bone Marrow Transpl. 1995;15(6):825–8.
17. Sullivan KM, Agura E, Anasetti C, Appelbaum F, Badger C, Bearman S, et al. Chronic graft-versus-host disease and other late complications of bone marrow transplantation. Semin Hematol. 1991;28(3):250–9.
18. Gooley TA, Leisenring W, Crowley J, Storer BE. Estimation of failure probabilities in the presence of competing risks: new representations of old estimators. Stat Med. 1999;18(6):695–706.
19. Storb R, Deeg HJ, Pepe M, Appelbaum F, Anasetti C, Beatty P, et al. Methotrexate and cyclosporine versus cyclosporine alone for prophylaxis of graft-versus-host disease in patients given HLA-identical marrow grafts for leukemia: long-term follow-up of a controlled trial. Blood. 1989;73(6):1729–34.
20. Deeg HJ, Lin D, Leisenring W, Boeckh M, Anasetti C, Appelbaum FR, et al. Cyclosporine or cyclosporine plus methylprednisolone for prophylaxis of graft-versus-host disease: a prospective, randomized trial. Blood. 1997;89(10):3880–7.
21. Ratanatharathorn V, Nash RA, Przepiorka D, Devine SM, Klein JL, Weisdorf D, et al. Phase III study comparing methotrexate and tacrolimus (prograf, FK506) with methotrexate and cyclosporine for graft-versus-host disease prophylaxis after HLA-identical sibling bone marrow transplantation. Blood. 1998;92(7): 2303–14.
22. Ferrara JL, Levine JE, Reddy P, Holler E. Graft-versus-host disease. Lancet. 2009;373(9674):1550–61.
23. Van Der Meer IM, De Maat MP, Hak AE, Kiliaan AJ, Del Sol AI, Van Der Kuip DA, et al. C-reactive protein predicts progression of atherosclerosis measured at various sites in the arterial tree: the Rotterdam Study. Stroke. 2002;33(12):2750–5.
24. Haverkate F, Thompson SG, Pyke SD, Gallimore JR, Pepys MB. Production of C-reactive protein and risk of coronary events in stable and unstable angina. European Concerted Action on Thrombosis and Disabilities Angina Pectoris Study Group. Lancet. 1997;349(9050):462–6.
25. Pasceri V, Willerson JT, Yeh ET. Direct proinflammatory effect of C-reactive protein on human endothelial cells. Circulation. 2000;102(18):2165–8.
26. Devaraj S, Davis B, Simon SI, Jialal I. CRP promotes monocyte-endothelial cell adhesion via Fcgamma receptors in human aortic endothelial cells under static and shear flow conditions. Am J Physiol Heart Circ Physiol. 2006;291(3):H1170–6.
27. Recalcati S, Invernizzi P, Arosio P, Cairo G. New functions for an iron storage protein: the role of ferritin in immunity and autoimmunity. J Autoimmun. 2008;30(1–2):84–9.
28. Matzner Y, Hershko C, Polliack A, Konijn AM, Izak G. Suppressive effect of ferritin on in vitro lymphocyte function. Br J Haematol. 1979;42(3):345–53.
29. Broxmeyer HE, Cooper S, Levi S, Arosio P. Mutated recombinant human heavy-chain ferritins and myelosuppression in vitro and in vivo: a link between ferritin ferroxidase activity and biological function. Proc Natl Acad Sci USA. 1991;88(3):770–4.
30. Cardier J, Romano E, Soyano A. Effect of hepatic isoferritins from iron overloaded rats on lymphocyte proliferative response: role of ferritin iron content. Immunopharmacol Immunotoxicol. 1995;17(4):719–32.
31. Gray CP, Franco AV, Arosio P, Hersey P. Immunosuppressive effects of melanoma-derived heavy-chain ferritin are dependent on stimulation of IL-10 production. Int J Cancer. 2001;92(6): 843–50.
32. Gray CP, Arosio P, Hersey P. Heavy chain ferritin activates regulatory T cells by induction of changes in dendritic cells. Blood. 2002;99(9):3326–34.
33. St Pierre TG, Clark PR, Chua-anusorn W, Fleming AJ, Jeffrey GP, Olynyk JK, et al. Noninvasive measurement and imaging of liver iron concentrations using proton magnetic resonance. Blood. 2005;105(2):855–61.

Leukemia (2012), 1–4

www.nature.com/leu

LETTER TO THE EDITOR

Direct binding of Grb2 has an important role in the development of myeloproliferative disease induced by ETV6/FLT3

Leukemia advance online publication, 14 December 2012; doi:10.1038/leu.2012.333

FMS-like tyrosine kinase 3 (*FLT3*) is one of the most frequently mutated genes in hematological malignancies.[1] The most common mutations of *FLT3* are internal tandem duplications (ITDs) within the juxtamembrane domain, which occur in 20% to 30% of patients with acute myeloid leukemia (AML).[2,3] Although FLT3 is a potential therapeutic target in AML, recent studies involving FLT3 inhibitors as single agents in patients with AML showed limited clinical responses.[4] FLT3 has been reported to fuse to ETV6 (TEL) in a few cases of myeloid/lymphoid neoplasms with eosinophilia (MLN-eo) carrying a translocation t(12;13)(p13;q12).[5,6] Although it has been shown that ETV6/FLT3 acts as a constitutively active tyrosine kinase, the molecular mechanisms underlying ETV6/FLT3-mediated leukemogenesis remain incompletely understood.[7–9]

We identified a novel *ETV6/FLT3* variant fusion transcript (E/F-1) in a MLN-eo patient (Supplementary Figures S1A and B) and investigated the transforming properties of ETV6/FLT3 *in vivo* using a murine bone marrow transplant (BMT) model.[10,11] E/F-1-transduced recipients developed an aggressive polyclonal myeloproliferative disease (MPD) in 100% of recipient mice with a latency of 3-4 weeks, as evidenced by marked leukocytosis, splenomegaly and massive expansion of myeloid cells in peripheral blood, spleen and bone marrow (Figures 1A–C). In this mice model, eosinophilia was not observed. Flow cytometric analysis of the peripheral blood from E/F-1 mice showed a large population of $EGFP^+/Mac\text{-}1^+/Gr\text{-}1^+$ cells. In primary E/F-1 mice, serial passage was performed by transferring a 1:1 mixture of spleen and bone marrow cells to sublethally irradiated recipient mice. This resulted in hematopoietic malignancies in most of the recipient mice receiving five different primary tumors. For three of the primary tumors, it was possible to transmit the MPD for at least one round. In all cases of serial passage, the MPD transformed into aggressive T-lymphoblastic lymphoma (T-LBL) with a latency of 4–17 weeks (Figure 1E, Supplementary Figure S2B). Most lymphoma occurred in the thymus or abdominal lymph nodes, and some of the secondary recipient mice displayed leukocytosis, generalized lymphadenopathy or hepatosplenomegaly. Histopathological examination revealed that the architecture of the lymph nodes and the thymus was completely effaced and that they contained a uniform population of lymphoblasts. The liver showed prominent periportal, lobular and sinusoidal infiltration by lymphoma cells (Figure 1D). Flow cytometric analysis of spleen cells revealed that the lymphomas typically showed an immature T-cell immunophenotype characterized by expression of both CD4 and CD8 (Supplementary Figure S2A). Affected tissues from secondary diseased mice contained proviral integrations identical to those in the primary MPD mouse (Figure 1F). ETV6/FLT3-induced T-LBL was transplantable, with all tertiary transplant recipients rapidly succumbing to T-LBL at 4–7 weeks after transfer arising from common clones identified in the secondary mice (Supplementary Figure S2C).

Previous studies have shown that FLT3-ITDs induce a lethal MPD in mice and that tyrosine residues 589 and 591 in the juxtamembrane domain of FLT3 are critical for STAT5 phosphorylation and generation of the MPD phenotype.[10] We also demonstrated the corresponding results for FLT3-ITD in our murine BMT experiment (Supplementary Figures S3A and B). On the other hand, mice that received the double tyrosine-to-phenylalanine mutant of E/F-1 at sites 589 and 591 (Y589/591F) in the juxtamembrane domain of FLT3 developed a similar MPD (Supplementary Table S1). There was no significant difference in survival between recipients of E/F-1 vs Y589/591F, with both mice groups succumbing to a fatal MPD within a median survival time of 18 and 19.5 days, respectively ($P = 0.284$; Figure 1C). The Y589/591F mutation did not abrogate STAT5, Erk1/2 and Akt activation in Ba/F3 cells transformed by E/F-1 (Supplementary Figure S4), which is consistent with the previous studies using a deletion mutant of the FLT3 juxtamembrane domain in ETV6/FLT3.[9]

Growth factor receptor-binding protein 2 (Grb2) is an adaptor protein known to bind several receptor tyrosine kinases. Grb2 binds the scaffolding protein Grb2-associated binder 2 (Gab2) and contributes to survival signaling in ligand-activated wild-type FLT3.[12] A recent study has shown that tyrosines 768, 955 and 969 of FLT3 are the direct Grb2-binding sites of importance for FLT3-ITD-mediated proliferation and survival of hematopoietic cells *in vitro* as a result of STAT5 activation via Gab2.[13] However, there have been no reports regarding the *in vivo* effects of direct Grb2 binding by oncogenic FLT3 in leukemogenesis. Thus, we investigated the role of Grb2 binding in ETV6/FLT3-mediated leukemogenesis. Inspection of the ETV6 portion of the fusion protein revealed only two candidate tyrosines for direct binding of Grb2 at positions 314 and 354. To test whether Grb2 binds directly to ETV6/FLT3, we made a series of Grb2-binding mutants of ETV6/FLT3 (Figure 2a). The Y314/354F double point mutant (2F) and the Y768/955/969F triple mutant (3F-1) of E/F-1 showed a reduced ability to bind Grb2 as compared with the E/F-1. Furthermore, when we mutated tyrosines 314 or 354 to phenylalanine in the context of the Y768/955/969F triple mutant, the association of ETV6/FLT3 with Grb2 was significantly reduced as compared with the Y768/955/969F triple mutant. Finally, when we mutated all five specific tyrosines (Y314/354/768/955/969) to phenylalanine, we observed that ETV6/FLT3 was no longer able to bind Grb2 (Figure 2b). Simultaneous mutation of these five tyrosine residues resulted in an absence of Gab2 phosphorylation, and impaired activation of STAT5, Erk1/2 and Akt in Ba/F3 cells (Figure 2c). ETV6/FLT3 variant E/F-2, which lacked the Grb2-binding sites of ETV6, was unable to bind to Grb2 when all three Grb2-binding sites of FLT3 were mutated (Figure 2b). This Y768/955/969F triple mutant of E/F-2 (3F-2) was also unable to phosphorylate Gab2 and showed weaker activation of STAT5, Erk1/2 and Akt as compared with E/F-2 in Ba/F3 cells (Figure 2c). Both E/F-1 and E/F-2 transformed bone marrow cells to be capable of cytokine-independent growth in methylcellulose medium. Transformation was significantly decreased in the 5F and 3F-2 mutants, which

Accepted article preview online 20 November 2012

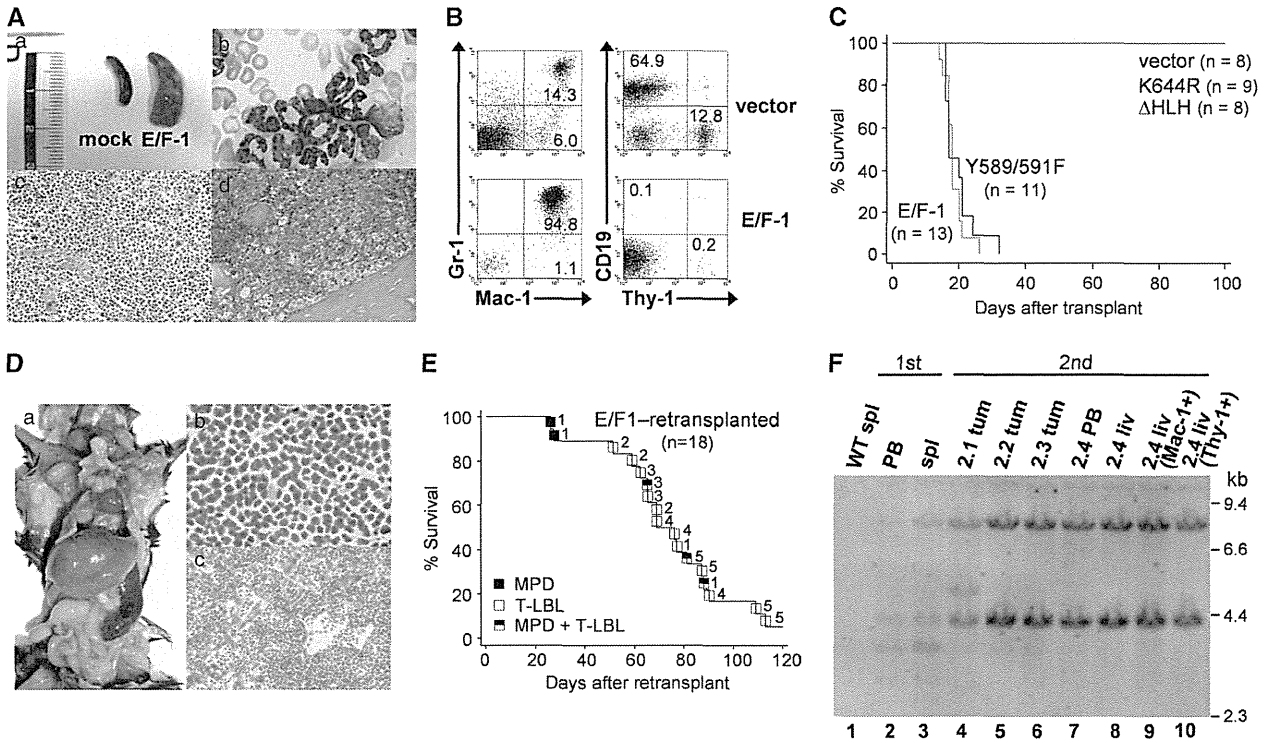

Figure 1. ETV6/FLT3 induces a rapidly fatal MPD in primary recipient mice, which transformed into T-LBL and MPD during serial passage. (**A**) (a) Splenomegaly associated with MPD. (b) Representative May–Giemsa-stained peripheral blood smear of the diseased mouse (× 100). (c, d) Representative hematoxylin and eosin-stained bone marrow (c) and spleen (d) of the diseased mouse (× 20). (**B**) Flow cytometric analysis of cells from the peripheral blood of vector control and E/F-1 mice. The percentages of cells in quadrants of interest are shown. (**C**) Survival curve for recipients of bone marrow transduced with a vector control ($n=8$), E/F-1 ($n=13$), Y589/591F mutant ($n=11$), kinase-inactive K644R mutant ($n=9$) or deletion mutant of the HLH oligomerization domain of ETV6 (ΔHLH) ($n=8$). Mice transplanted with a vector control, K644R, or ΔHLH remain free of disease 180 days after transplant. Survival data are cumulative from two or three separate experiments for all retroviral constructs. (**D**) (a) Macroscopic examination of a secondary recipient with T-LBL (b and c) Hematoxylin and eosin-stained lymph node (b) and liver (c) of the diseased mouse (× 100 and × 20, respectively). (**E**) Kaplan–Meier survival analysis of the secondary recipients. Most secondary recipients succumbed to T-LBL or/and MPD. Pairs of recipients transplanted with cells from the same primary donor are indicated by numbers. (**F**) Proviral integrations in cells isolated from primary and secondary recipients. Genomic DNA isolated from the indicated tissues of a wild-type (WT) mouse (lane 1), a primary MPD mouse (lanes 2 and 3) and four secondary T-LBL mice receiving bone marrow and spleen from the same primary MPD mouse (lanes 4–10) was digested with *Eco*RI and analyzed for proviral integrations by hybridization with a DIG-labeled EGFP probe. Lanes 4–6 are DNAs from the tumors of mice with T-LBL. Lanes 7–10 represent lineage analysis from a single secondary mouse, which developed both MPD and T-LBL (2.4). The peripheral blood of the 2.4 mouse contained 83.5% EGFP$^+$Mac-1$^+$ and 10.6% EGFP$^+$Thy-1$^+$ cells, and the liver of the 2.4 mouse contained 27.2% EGFP$^+$Mac-1$^+$ and 58.8% EGFP$^+$Thy-1$^+$ cells at the time of euthanization. The MACS-sorted liver myeloid (Mac-1$^+$) and T cells (Thy-1$^+$) from this mouse were 98.1% and 98.4% pure, respectively. DNA size markers (in kb) are shown on the right. liv, liver; PB, peripheral blood; spl, spleen; tum, tumor.

were unable to bind Grb2, but not in 2F and 3F-1 mutants (Figure 2d). To examine the contribution of Grb2 binding to ETV6/FLT3-induced MPD *in vivo*, we performed BMT experiments. White blood cell (WBC) counts and spleen weights of the mice receiving 5F-transduced bone marrow were significantly lower than those receiving E/F-1-transduced bone marrow (Supplementary Table S1). Flow cytometric analyses of spleen cells showed that 5F mice had a reduced fraction of Mac-1$^+$/Gr-1$^+$ cells compared with E/F-1 mice (Supplementary Figure S5A). 5F mice showed significantly less infiltrate in the hepatic lobules or periportal areas than the E/F-1 mice (Supplementary Figure S5B). Recipients of both 2F and 3F-1 developed rapidly fatal MPD with a comparable latency to those of E/F-1. Survival of 5F and 3F-2 mice was significantly prolonged compared with that of E/F-1 and E/F-2 mice, respectively (55 days vs 18 days, 73 days vs 13 days, respectively; $P<0.001$; Figure 2e), although most 5F and 3F-2 recipient mice eventually succumbed to MPD.

Finally, we compared the ability of ETV6/FLT3 to transform primary myeloid cells from the bone marrow of Gab2$^{-/-}$ and Gab2$^{+/+}$ mice. Expression of E/F-1 in Gab2$^{-/-}$ cells resulted in an approximately threefold lower number of cytokine-independent CFU-C (Supplementary Figure S6A). We assessed the relative contribution of the *Gab2* gene to ETV6/FLT3-mediated leukemogenesis in BMT experiments using Gab2$^{-/-}$ and Gab2$^{+/+}$ donor mice. All mice transplanted with Gab2$^{+/+}$ bone marrow cells expressing ETV6/FLT3 developed severe MPD (median WBC, $236\times10^3/\mu l$; spleen weight, 561 mg), as expected (Supplementary Figure S6B). ETV6/FLT3-induced myeloproliferation was attenuated in mice transplanted with Gab2$^{-/-}$ bone marrow cells expressing ETV6/FLT3 (median WBC, $31\times10^3/\mu l$; spleen weight, 350 mg). Survival of mice injected with Gab2$^{-/-}$ bone marrow cells expressing E/F-1 was significantly prolonged in comparison with those injected with Gab2$^{+/+}$ cells (56 days vs 21 days, $P<0.001$; Figure 2f), although all recipients of Gab2$^{-/-}$ background bone marrow cells eventually succumbed to MPD.

Our results suggest that ETV6/FLT3 has more potent oncogenic activity than FLT3-ITDs and can transform progenitor cells with the capacity to differentiate into myeloid and lymphoid progeny, supporting the contention that human *ETV6/FLT3*-positive MLN-eo is a stem cell disorder. Unlike FLT3-ITDs, mice that received the

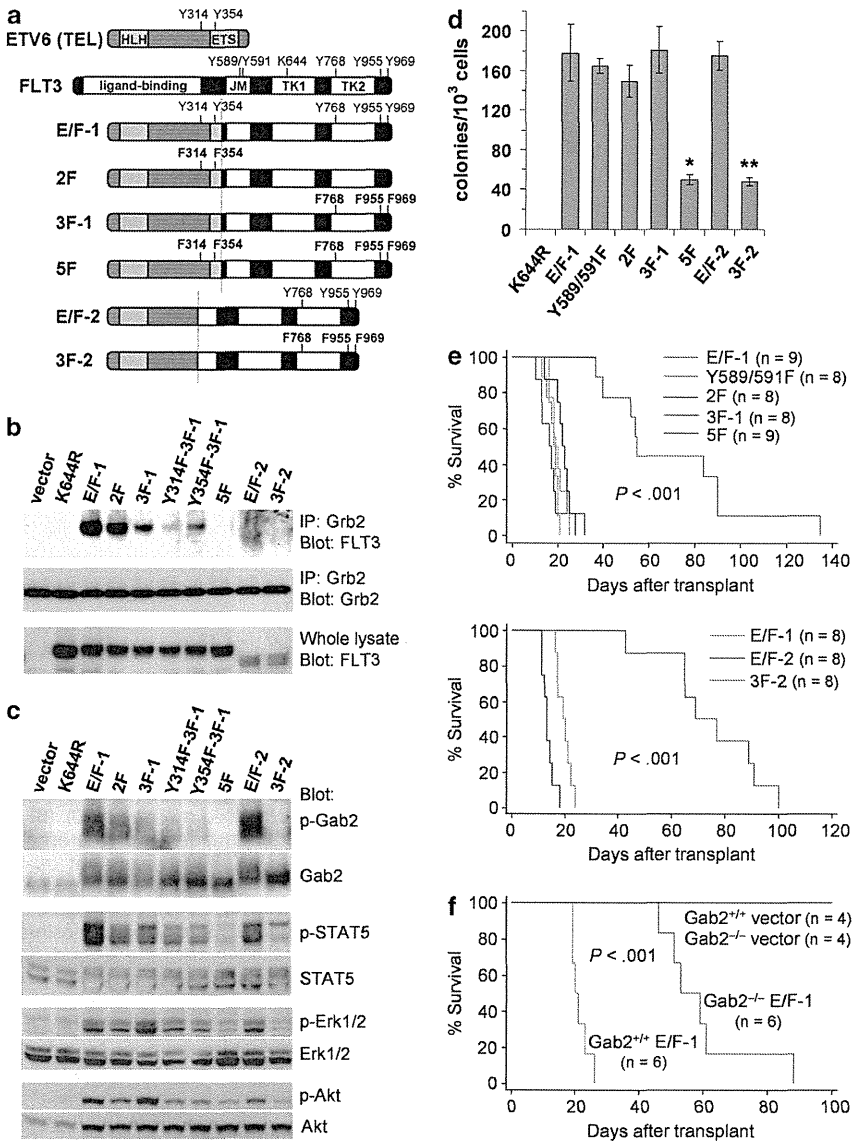

Figure 2. Both ETV6 and FLT3 portions contribute to ETV6/FLT3-mediated leukemogenesis via Grb2-Gab2 pathway. (**a**) Schematic representation of ETV6/FLT3 fusion proteins including the series of Grb2-binding site mutants. The point of fusion is indicated by a vertical dotted line. E/F-1 was cloned by us. E/F-2 was cloned previously (Vu *et al.*[5]). (**b**) Coimmunoprecipitation: lysates from Ba/F3 cells expressing the indicated ETV6/FLT3 proteins were immunoprecipitated using an anti-Grb2 antibody and blotted with anti-FLT3 (top) and anti-Grb2 (middle) antibodies. Whole-cell lysates were also blotted with the anti-FLT3 antibody (bottom). As a control, lysates from vector-transduced cells were included. Three independent experiments were performed and representative data are shown. (**c**) Activation of downstream targets was demonstrated by blotting the whole-cell lysates of Ba/F3 cells with the indicated phosphospecific antibodies. After stripping, the membranes were reprobed with the indicated total antibodies. Three independent experiments were performed and representative data are shown. (**d**) Cytokine-independent colony formation of whole bone marrow cells expressing ETV6/FLT3 wild-type or Grb2-binding mutants. The difference between E/F-1 and 5F (*) and between E/F-2 and 3F-2 (**) is statistically significant ($P<0.001$, unpaired *t*-test). Data are the mean ± s.d. of three independent experiments. (**e**) Survival curve for recipients of bone marrow transduced with ETV6/FLT3 and Grb2-binding mutants. Both E/F-1 and E/F-2 mice caused rapidly fatal MPD. 5F mutant mice and 3F-2 mutant mice developed MPD with a longer median survival of 55 and 73 days, respectively ($P<0.001$ vs E/F-1 and E/F-2, respectively). One of the 5F mutant mice died of severe anemia without showing any signs of MPD. Survival data are cumulative from two or three separate experiments for all retroviral constructs. (**f**) Survival curve for recipients of $Gab2^{-/-}$ and $Gab2^{+/+}$ bone marrow transduced with a vector control or E/F-1. The *P*-value represents a comparison of survival by E/F-1 on $Gab2^{-/-}$ vs $Gab2^{+/+}$ background.

Y589/591F mutant of ETV6/FLT3 also developed a lethal MPD with a short latency. The reason for the discrepancy between ETV6/FLT3 and FLT3-ITDs is not clear. This may be due to altered structural conformation of ETV6/FLT3 relative to wild-type FLT3 or alternatively, it may be due to different subcellular localization of the fusion protein and FLT3-ITDs.[14,15] Recently it was reported that sunitinib and sorafenib, tyrosine kinase inhibitors with multiple targets including FLT3, had therapeutic efficacy in two patients with *ETV6/FLT3*-positive MLN-eo.[6] Unfortunately, similar to most of the patients with *FLT3-ITD*-positive AML, relapse and resistance occurred in both patients. Although clinical application of Grb2 inhibitors remains limited to just a phase I trial of a liposomal antisense for hematological malignancies, the results of the current study indicate therapeutic potential against Grb2 in

patients with *ETV6/FLT3*-positive MLN-eo. In addition, previous studies have shown that the Grb2-Gab2 pathway also has an important role in FLT3-ITD-mediated cell proliferation and survival.[13,15] These findings suggest that inhibition of this pathway may be useful in the treatment of FLT3-associated leukemia.

CONFLICT OF INTEREST

The authors declare no conflict of interest.

ACKNOWLEDGEMENTS

This work was supported in part by grants from the Ministry of Education, Culture, Sports, Science and Technology of Japan (MH).

K Chonabayashi[1], M Hishizawa[1], S Kawamata[2], Y Nagai[1], T Ohno[3], T Ishikawa[1], T Uchiyama[1] and A Takaori-Kondo[1]
[1]*Department of Hematology and Oncology, Graduate School of Medicine, Kyoto University, Kyoto, Japan;*
[2]*Foundation for Biomedical Research and Innovation, Kobe, Japan and*
[3]*Division of Hematology and Immunology, Department of Internal Medicine, Ohtsu Red Cross Hospital, Ohtsu, Japan*
E-mail: hishiza@kuhp.kyoto-u.ac.jp

REFERENCES

1 Stirewalt DL, Radich JP. The role of FLT3 in haematopoietic malignancies. *Nat Rev Cancer* 2003; **3**: 650–665.
2 Kiyoi H, Naoe T, Nakano Y, Yokota S, Minami S, Miyawaki S *et al.* Prognostic implication of FLT3 and N-RAS gene mutations in acute myeloid leukemia. *Blood* 1999; **93**: 3074–3080.
3 Thiede C, Steudel C, Mohr B, Schaich M, Schakel U, Platzbecker U *et al.* Analysis of FLT3-activating mutations in 979 patients with acute myelogenous leukemia: association with FAB subtypes and identification of subgroups with poor prognosis. *Blood* 2002; **99**: 4326–4335.
4 Kindler T, Lipka DB, Fischer T. FLT3 as a therapeutic target in AML: still challenging after all these years. *Blood* 2010; **116**: 5089–5102.
5 Vu HA, Xinh PT, Masuda M, Motoji T, Toyoda A, Sakaki Y *et al.* FLT3 is fused to ETV6 in a myeloproliferative disorder with hypereosinophilia and a t(12;13)(p13;q12) translocation. *Leukemia* 2006; **20**: 1414–1421.
6 Walz C, Erben P, Ritter M, Bloor A, Metzgeroth G, Telford N *et al.* Response of ETV6-FLT3-positive myeloid/lymphoid neoplasm with eosinophilia to inhibitors of FMS-like tyrosine kinase 3. *Blood* 2011; **118**: 2239–2242.
7 Tse KF, Mukherjee G, Small D. Constitutive activation of FLT3 stimulates multiple intracellular signal transducers and results in transformation. *Leukemia* 2000; **14**: 1766–1776.
8 Baldwin BR, Li L, Tse KF, Small S, Collector M, Whartenby KA *et al.* Transgenic mice expressing Tel-FLT3, a constitutively activated form of FLT3, develop myeloproliferative disease. *Leukemia* 2007; **21**: 764–771.
9 Vu HA, Xinh PT, Kano Y, Tokunaga K, Sato Y. The juxtamembrane domain in ETV6/FLT3 is critical for PIM-1 up-regulation and cell proliferation. *Biochem Biophys Res Commun* 2009; **383**: 308–313.
10 Rocnik JL, Okabe R, Yu JC, Lee BH, Giese N, Schenkein DP *et al.* Roles of tyrosine 589 and 591 in STAT5 activation and transformation mediated by FLT3-ITD. *Blood* 2006; **108**: 1339–1345.
11 Tanaka Y, Era T, Nishikawa S, Kawamata S. Forced expression of Nanog in hematopoietic stem cells results in a gammadeltaT-cell disorder. *Blood* 2007; **110**: 107–115.
12 Zhang S, Broxmeyer HE. Flt3 ligand induces tyrosine phosphorylation of gab1 and gab2 and their association with shp-2, grb2, and PI3 kinase. *Biochem Biophys Res Commun* 2000; **277**: 195–199.
13 Masson K, Liu T, Khan R, Sun J, Ronnstrand L. A role of Gab2 association in Flt3 ITD mediated Stat5 phosphorylation and cell survival. *Br J Haematol* 2009; **146**: 193–202.
14 Schmidt-Arras DE, Bohmer A, Markova B, Choudhary C, Serve H, Bohmer FD. Tyrosine phosphorylation regulates maturation of receptor tyrosine kinases. *Mol Cell Biol* 2005; **25**: 3690–3703.
15 Choudhary C, Olsen JV, Brandts C, Cox J, Reddy PN, Bohmer FD *et al.* Mislocalized activation of oncogenic RTKs switches downstream signaling outcomes. *Mol Cell* 2009; **36**: 326–339.

Supplementary Information accompanies this paper on the Leukemia website (http://www.nature.com/leu)

SCIENTIFIC REPORTS

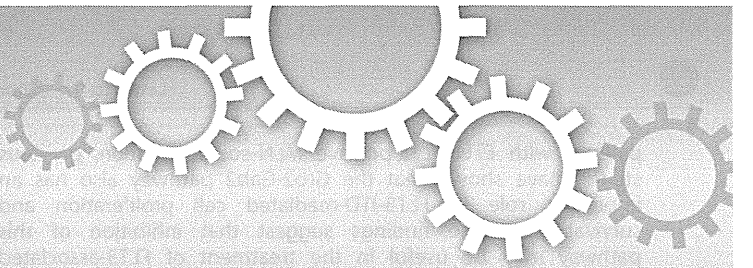

SUBJECT AREAS:
CANCER GENOMICS
HAEMATOLOGICAL CANCER
DNA DAMAGE AND REPAIR
ONCOGENES

Received
2 August 2012

Accepted
10 October 2012

Published
13 November 2012

Correspondence and requests for materials should be addressed to K.S. (shind009@kuhp.kyoto-u.ac.jp)

APOBEC3B can impair genomic stability by inducing base substitutions in genomic DNA in human cells

Masanobu Shinohara, Katsuhiro Io, Keisuke Shindo, Masashi Matsui, Takashi Sakamoto, Kohei Tada, Masayuki Kobayashi, Norimitsu Kadowaki & Akifumi Takaori-Kondo

Department of Hematology and Oncology, Graduate school of medicine, Kyoto University, Kyoto 606-8507, Japan.

Human APOBEC3 proteins play pivotal roles in intracellular defense against viral infection by catalyzing deamination of cytidine residues, leading to base substitutions in viral DNA. Activation-induced cytidine deaminase (AID), another member of the APOBEC family, is capable of editing immunoglobulin (Ig) and non-Ig genes, and aberrant expression of AID leads to tumorigenesis. However, it remains unclear whether APOBEC3 (A3) proteins affect stability of human genome. Here we demonstrate that both A3A and A3B can induce base substitutions into human genome as AID can. A3B is highly expressed in several lymphoma cells and somatic mutations occur in some oncogenes of the cells highly expressing A3B. Furthermore, transfection of *A3B* gene into lymphoma cells induces base substitutions in *cMYC* gene. These data suggest that aberrant expression of A3B can evoke genomic instability by inducing base substitutions into human genome, which might lead to tumorigenesis in human cells.

It is widely recognized that the accumulation of genetic changes in tumor-related genes is essential for cancer development[1]. With the innovation of high-throughput sequencing technology, genome-wide analyses on various types of cancer cells have revealed numerous somatic mutations in tumor-related genes[2]. Some of these mutations are caused by defects in DNA repair systems (e.g., DNA mismatch repair deficiencies give rise to hereditary non-polyposis colon cancer[3]), whereas mechanisms that account for the majority of genetic changes in cancer cells are poorly understood. Referring to somatic base substitution spectra in cancer cells, C/G to T/A transitions are most prevalent, especially in gastric cancer, colorectal cancer, glioma, and melanoma[2,4,5]. This strong bias in somatic mutations suggests the existence of active mechanisms that induce C/G to T/A transitions into genomic DNA. It is obviously attributable to ultraviolet irradiation and following repair process against pyrimidine dimer in case of melanoma, but not in others.

The human APOBEC family proteins can induce C to T (G to A, in complementary sequences) transitions into target DNA through cytidine deamination. The APOBEC family is comprised of a series of molecules with conserved cytidine deaminase domains (CDAs), including AID, APOBEC1, APOBEC2, APOBEC3A to H, and APOBEC4[6,7]. Among them, AID plays a crucial role in somatic hypermutation and class switch recombination of Ig genes, which enables diversification of immune system[8]. AID has been considered the only molecule that can induce C/G to T/A transitions into genomic DNA. The expression of AID is highly regulated and restricted in germinal center B-cells under physiological conditions, but with inflammatory stimulations, AID can be overexpressed in not only B-cells but also other types of cells (e.g., epithelial cells) via activation of NF-κB[9]. Aberrant expression of AID results in the accumulation of mutations in non-Ig genes[10], which leads to development of various cancers such as gastric and hepatic cancers as well as lymphomas[9,11–13].

A series of seven A3 genes are tandemly arrayed on human chromosome 22, and the main function of the resulting gene products is to protect the cells from retroviruses and endogenous mobile retroelements[14,15]. A3B, A3D, A3F, and A3G contain two CDAs, instead of one in A3A, A3C, and A3H. A3G is a powerful anti-retroviral molecule that induces cytidine deamination in viral genome and acts as a host defensive factor against viruses such as HIV-1[16]. A3A and A3B have been reported as potent inhibitors of retrotransposons[17]. Thus, A3 proteins act as sentinels in innate immunity against mobile DNA/RNA including viruses, while little is known about the effect of these proteins on nuclear DNA, in other words, host human genome. Recent studies have demonstrated that A3A impairs nuclear DNA under the condition of suppressing uracil DNA-glycosylase (UNG) which prevents base alterations by eliminating uracil from DNA and initiating the base-excision repair pathway[18,19].

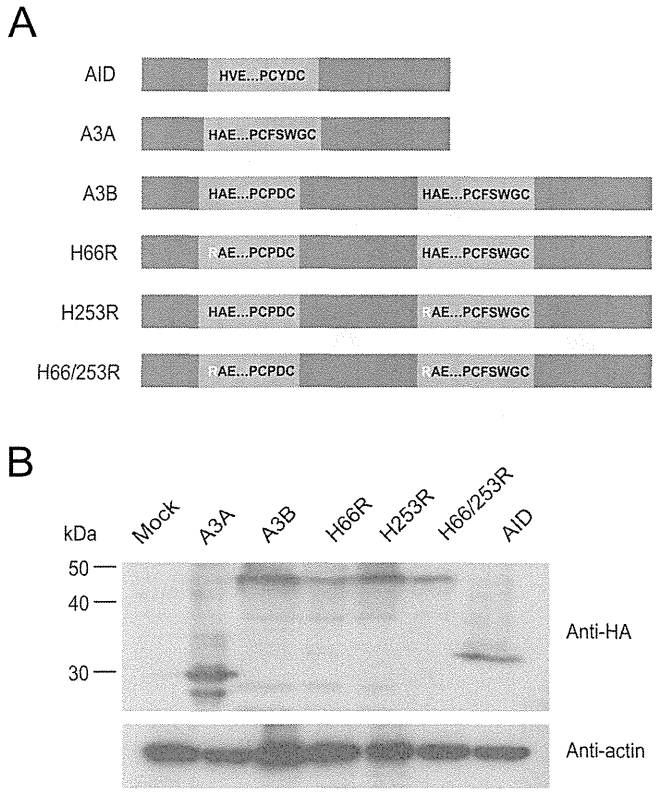

Figure 1 | Expression of A3A, A3B wild-type and mutants, and AID. (A) Schematic of expression vectors. The consensus amino acid residues for zinc-coordinating motifs are shown. Substituted residues are shown in white. (B) Expression of HA-tagged proteins. Expression vectors were transfected into HEK293 cells, and cell lysates were analyzed by immunoblotting with anti-HA antibody (top panel) and anti-ß-actin antibody (bottom panel) for loading control.

However, it is still unclear whether A3 proteins can induce somatic mutations into human genome with intact DNA repair systems. Here we first demonstrate that expression of A3B and A3A as well as AID can induce somatic mutations in genomic DNA in human cells even in the presence of UNG. We also find that high expression of A3B leads to somatic mutations in tumor-related genes. These data suggest that aberrant expression of A3B might be one of the active mechanisms that induce somatic mutations in cancer cells.

Results

A3 and AID induce hypermutations into foreign DNA. Besides A3A, we focused on A3B because it is localized predominantly in the nucleus[20,21] and highly expressed in many types of cancer cells[14] referring to microarray database (e.g., NextBio: http://www.nextbio.com). Previous studies have shown that A3B contains two enzymatically active CDAs in restricting HIV-1[22], whereas only carboxyl-terminal CDA is responsible for inhibiting HBV replication[23,24] and editing bacterial DNA[22]. A3B is also shown to restrict foreign DNA in mammalian cells[25], but it has not been tested which CDA is active in this context. First, to examine whether A3 and AID induce mutations in foreign DNA in human cells and which CDA is responsible for this DNA editing, we constructed amino- and/or carboxyl-terminal CDA mutants (H66R, H253R, and H66/253R) by site directed mutagenesis (Fig. 1a) and confirmed their expression in HEK293 cells by immunoblotting (Fig 1b). We transfected expression vectors for these together with EGFP expression vector into HEK293 cells and examined base substitutions in *EGFP* sequences. The expression vector for UNG inhibitor (UGI) was also co-transfected to avoid UNG-triggered degradation of uracil-containing foreign DNA as described previously[25]. We recovered total DNA from the cells 2 days after transfection and performed differential DNA denaturation PCR (3D-PCR) to efficiently recover edited DNA sequences[26]. 3D-PCR is based on the principle that DNA sequences with fewer interstrand hydrogen bonds dissociates easier. If cytidine deamination takes place frequently, resulting AT-rich *EGFP* gene can be amplified at lower denaturation temperatures. Although PCR products were obtained from all samples at 92°C of denaturation temperature (Td), we obtained robust PCR products at 83.8°C of Td only from A3A-, A3B wild-type (WT)-, and AID-expressing cells (Fig 2a). Amplification of *EGFP* at the lowest Td was impaired in H66R-expressing cells compared to A3B WT-expressing cells and undetectable in H253R- or H66/253R-expressing cells (Fig 2a, bottom). To ascertain whether *EGFP* gene was actually hyperedited, we cloned and sequenced the amplicons at 83.8°C of Td. As can be seen from the mutation matrices, high levels of C/G to T/A transitions were introduced into *EGFP* sequences (Fig 2b). To compare the extent of baseline mutations and that of A3B-induced mutations, we also cloned and sequenced the amplicons at 94.0°C of Td. Mutation frequency of A3B-expressing cells were about 6 times higher than that of mock-transfected cells (Supplementary Fig. S1 online). The mutation frequency in H66R-expressing cells was approximately a half compared to that in A3B WT-expressing cells in the amplicons at the lowest Td (Fig 2c). These data suggest that carboxyl-terminal CDA of A3B is mainly responsible for foreign DNA editing, but both domains are requisite for full editing activity. It is worth noting that AID is also capable of inducing cytidine deamination into foreign DNA.

Human A3 proteins have preferred target dinucleotide sequences in the substrate DNA; A3A and A3B prefer to deaminate cytosine residues flanked by 5′ thymine residue, 5′-TC, whereas A3G prefers to deaminate cytosine residues flanked by 5′ cytosine residue, 5′-CC[25,27–29]. We analyzed the context of C/G to T/A transitions in hyperedited *EGFP* sequences. We observed a strong bias toward deamination at 5′-TC dinucleotides in A3A-, A3B WT-, and H66R-expressing cells, but not in AID-expressing cells (Fig 2d). 5′-TC dinucleotide preference of A3B was also confirmed by sequencing amplicon at 94.0°C of Td which is supposed to be unbiased (Supplementary Fig. S1 online). These data suggest that the preference of editing sites in foreign DNA by A3s coincides with that seen in viral DNA.

A3A and A3B can edit genomic DNA in human cells. We next investigated whether A3 proteins induce C/G to T/A transitions into not only foreign DNA but also nuclear DNA in human cells. We first established a HEK293 cell line stably expressing EGFP (HEK293/EGFP) using retrovirus vector that carries *EGFP*. We transfected HEK293/EGFP cells with expression vectors for A3A, A3B WT or mutant (H66R, H253R, or H66/253R), or AID by lipofection, and then recovered total DNA from these cells after 7-day culture. We performed 3D-PCR of *EGFP* gene and obtained amplicons from A3A-, A3B WT-, H66R-, and AID-expressing cells at lower Td (Fig 3a). *EGFP* gene was recovered at Td as low as 86.3°C from A3B WT-expressing cells, while as low as 86.5°C from A3A-, H66R-, and AID-expressing cells. By contrast, *EGFP* gene was not amplified below Td of 87°C from cells transfected with mock, H253R or H66/253R. We repeated this procedure consisting of transfection, DNA extraction, and 3D-PCR three times and obtained similar results (Fig 3b). To unambiguously confirm the presence of C/G to T/A transitions, we cloned and sequenced amplicons obtained at the lowest Td in A3A-, A3B WT-, H66R-, and AID-expressing cells (Fig 3c). These analyses revealed approximately 2 to 5 C/G to T/A transitions per *EGFP* sequence from each sample (Fig 3d). The transitions were detected most frequently in A3A-expressing cells, and deaminase activity of H66R mutant was approximately a half

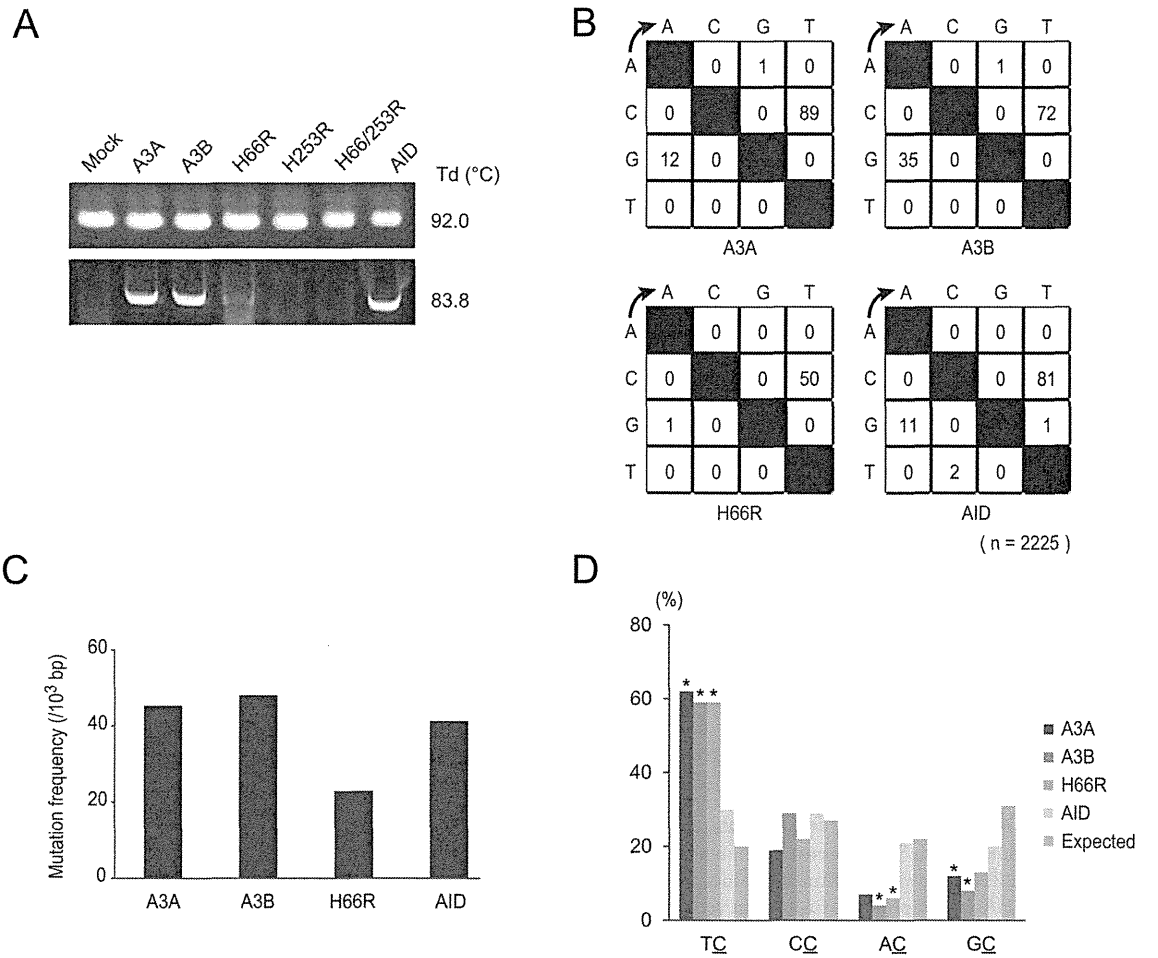

Figure 2 | Foreign DNA editing by A3A, A3B, and AID. (A) Agarose gel analyses of 3D-PCR products from HEK293 cells. Cells were transfected with expression vector for A3A, A3B wild-type or mutant, or AID together with pEGFP-N3 and pEF-UGI. Total DNA was recovered 2 days after transfection, and *EGFP* gene was amplified by 3D-PCR at the indicated denaturation temperatures (Td). (B) Mutation matrices of hyperedited *EGFP* sequences derived from cloned amplicons at 83.8°C of Td. "n" indicates the number of bases sequenced. We sequenced 5 clones (2,225 base pairs in total) in each group. (C) Frequencies of C/G to T/A transitions in hyperedited *EGFP* genes. C/G to T/A transitions per 1,000 sequenced base pairs are shown. (D) Dinucleotide contexts in foreign DNA editing. The rates of indicated dinucleotide sequence at the C to T transitions are shown. Asterisks indicate statistical significance in a χ^2 test ($p < 0.01$).

compared to that of A3B WT as seen in foreign DNA assays. The contexts of C/G to T/A transitions detected from the lowest Td amplicons in genomic DNA editing in A3-expressing cells were distinct from those in foreign DNA editing (Fig 3e). A preference for 5′-TC dinucleotide was not apparently observed, alternatively, 5′-GC dinucleotides were preferred in all samples. However, this bias fails to reach statistical significance ($p < 0.01$) in a χ^2 test. The preferred target sequences of AID editing were 5′-GC and 5′-AC dinucleotides as described by many prior studies[27,30]. Mutation frequencies and preferred target sequence of A3B was also analyzed by using amplicons at 94.0°C of Td. Mutation frequency of A3B-expressing cells were about 3 times higher than that of mock-transfected cells (Supplementary Fig. S2 online). A preference for 5′-TC dinucleotide was impaired, compared to that in foreign DNA editing assays (Supplementary Fig. S2 online). Our results reveal that in addition to AID, A3A and A3B can induce C/G to T/A transitions into human nuclear DNA without repressing proofreading enzymes (e.g., UNG). Mutation frequencies were 6 to 9 per 1000 base pairs in A3A-, A3B WT-, and AID-expressing cells, and much less frequent compared to those in foreign DNA editing. As seen with foreign DNA editing, carboxyl-terminal CDA is mainly responsible for catalytic activity but not sufficient for full editing activity. The preference context of genomic DNA editing by A3A and A3B is different from that of viral or foreign DNA editing.

Deep sequencing reveals hyperediting of human genomic DNA by A3 proteins. Amplicon sequencing by next-generation sequencer has enabled to detect extremely low levels of mutations of targeted regions in genomic DNA. To verify more certainly that A3 proteins edit human nuclear DNA, we performed deep sequencing of A3-expressing cells. HEK293/EGFP cells were transfected with an empty vector or expression vectors for A3A, A3B WT, H66/253R, or AID by lipofection, and total DNA were extracted after 7-day culture. We amplified a portion of *EGFP* gene with 443 base pair length (from thymine 56 to cytosine 498) by conventional PCR protocol, not by 3D-PCR, and performed amplicon sequencing with the coverage of 1337 to 2654 reads per sample. This analysis revealed that extremely large numbers of nucleotides were substituted over the full length of amplicons in A3A-, A3B WT-, and AID-expressing cells, whereas very few mutations were detected in mock and H66/253R-expressing cells (Supplementary Table 1 online). C/G to T/A transitions were observed most frequently in A3A-expressing cells as variation rates reach approximately 7% at the maximum, while below 3% at most in A3B- and AID-expressing cells (Fig 4a

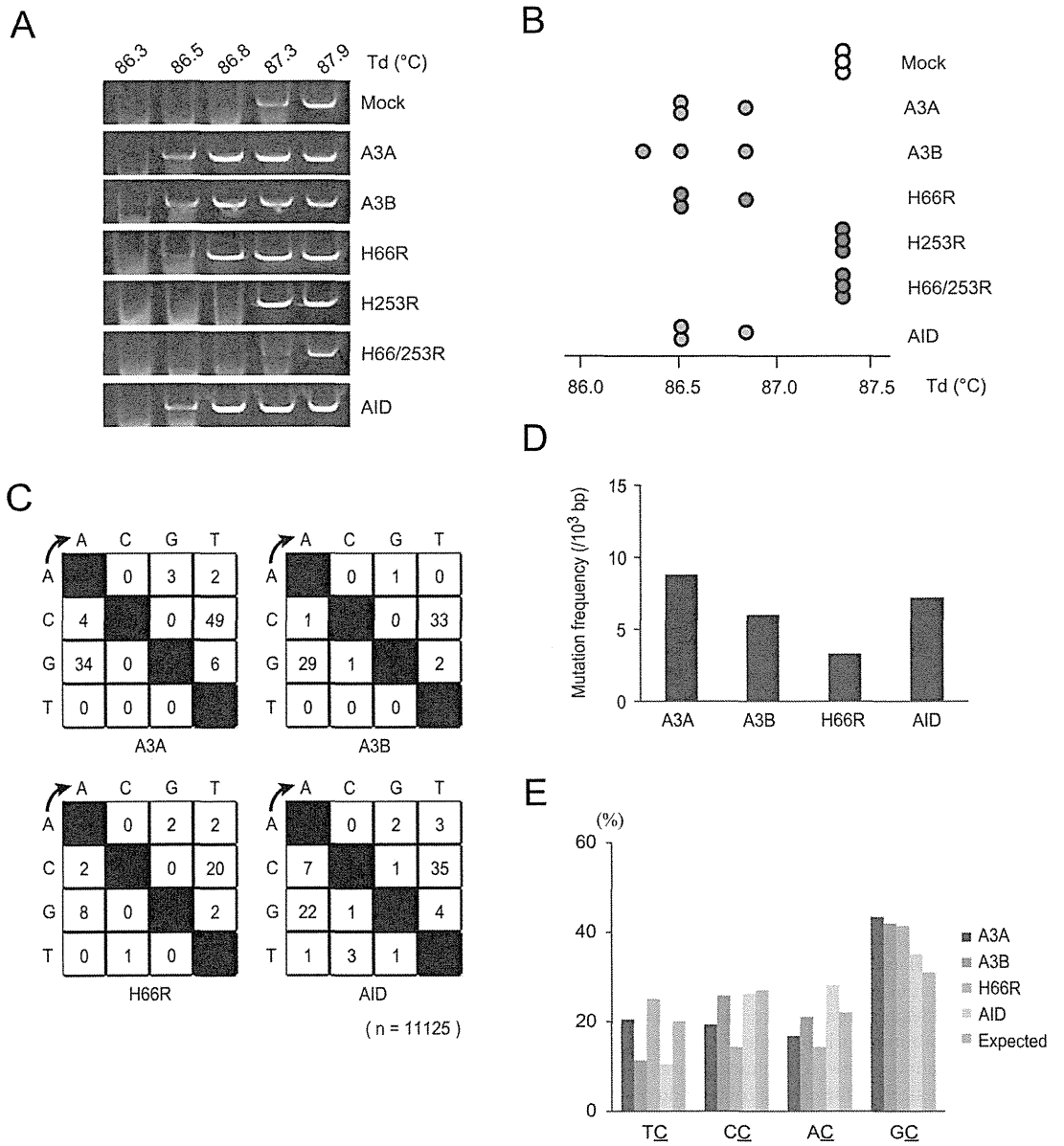

Figure 3 | Hypermutations in *EGFP* genes integrated in genomic DNA of HEK293 cells. (A) Agarose gel analyses of 3D-PCR products of *EGFP* genes extracted from HEK293/EGFP cells. Cells were transfected with expression vector for A3A, A3B wild-type or mutant, or AID. Total DNA was recovered 7 days after transfection and *EGFP* genes were amplified by 3D-PCR at the indicated denaturation temperatures (Td). (B) Distributions of the lowest denaturation temperatures for positive PCR amplification in each sample. Each circle represents independent experiment consisting of transfection, DNA extraction, and 3D-PCR. (C) Mutation matrices of hyperedited *EGFP* sequences derived from cloned PCR products at Td lower than 87°C. "n" indicates the number of bases sequenced. We sequenced 25 clones (11,125 base pairs in total) in each group. (D) Frequencies of C/G to T/A transitions in hyperedited *EGFP* genes. C/G to T/A transitions per 1,000 sequenced base pairs are shown. (E) Dinucleotide contexts in genomic DNA editing. The rates of indicated dinucleotide sequence at the C to T transitions are shown. Deviations in the editing contexts do not reach statistical significance ($p < 0.01$) in a χ^2 test.

and Supplementary Table 1 online). The mutation frequency analysis revealed that large numbers of C/G to T/A substitutions were induced in A3A-, A3B-, and AID-expressing cells, whereas other types of base substitutions were very few (Fig 4b). These results are similar to the data obtained by 3D-PCR and clonal sequencing of A3- and AID-expressing cells, and further demonstrated that A3A and A3B as well as AID can induce C/G to T/A transitions into genomic DNA in human cells with intact DNA repair systems. Dinucleotide preference of target sequence for deamination by A3A, A3B and AID was also analyzed, however, we did not found any preference in this experiment (Fig. 4C), suggesting the difference between foreign DNA editing and genomic DNA editing.

Expression of A3B and somatic mutations in lymphoma cells. Although AID has been reported to play important roles in lymphomagenesis by inducing mutations in both Ig and non-Ig genes[11,12,31–34], AID-independent mechanisms are also suggested, because AID is not expressed in all types of B-cell lymphomas[31,35]. We hypothesized that A3 may contribute to somatic mutations in some lymphoma cells. To examine this hypothesis, we first determined expression levels of *A3A*, *A3B*, and *AID* by quantitative RT-PCR in several B-cell lymphoma cell lines using peripheral blood lymphocytes (PBL) as control (Fig 5a). Our analysis revealed that *A3B* was highly expressed in 3 of 4 cell lines, particularly, markedly high in KIS1 cells, whereas expression of *A3A* transcripts was not detected in any

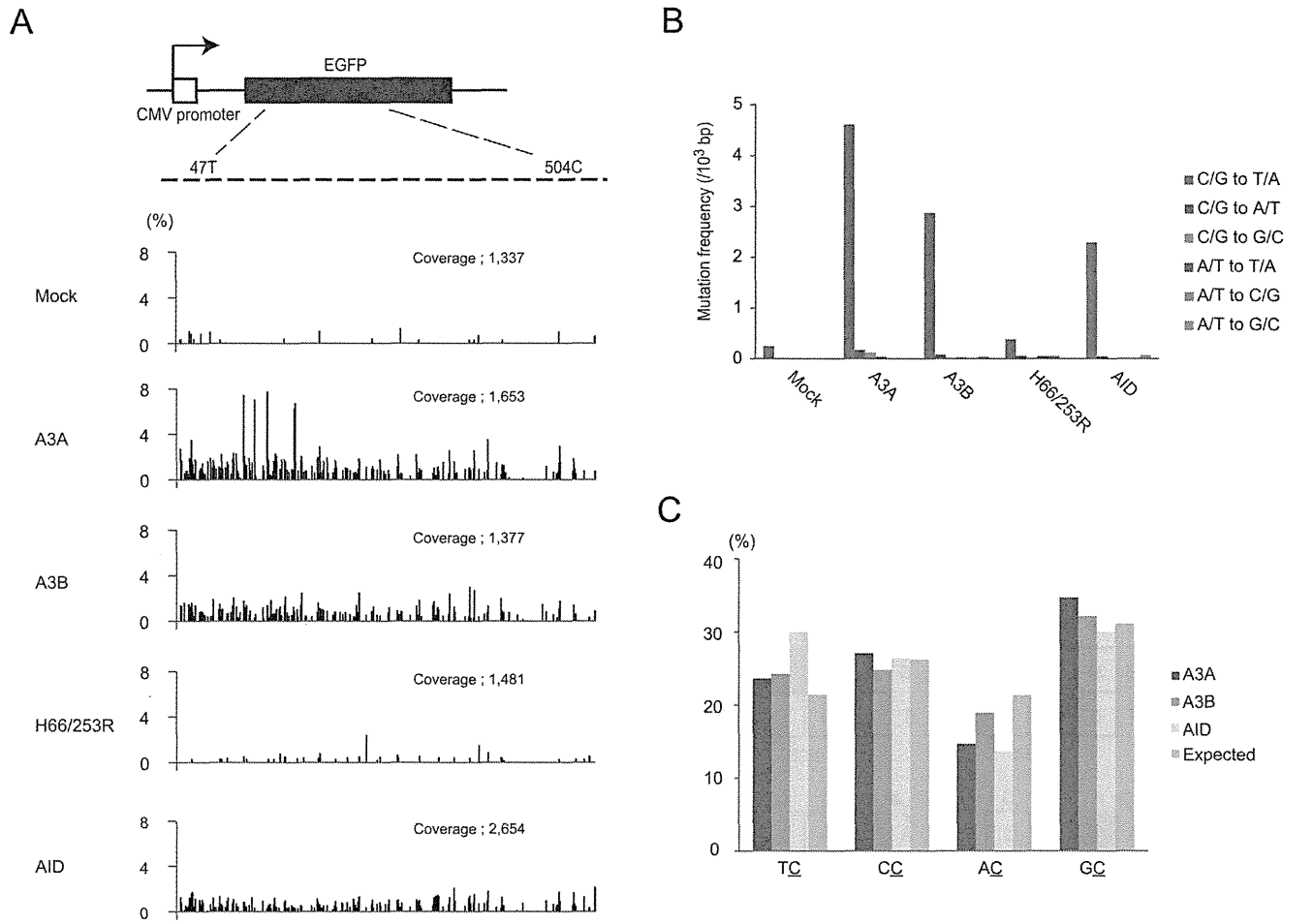

Figure 4 | Deep sequencing of *EGFP* genes in genomic DNA. (A) The distributions of C/G to T/A substitutions in the *EGFP* sequences. Total DNA was recovered form HEK293/EGFP cells 7 days after transfection with expression vector for A3A, A3B wild type or H66/253R or AID. We amplified a portion of *EGFP* sequence from thymine 47 to cytidine 504 (top schematic) by PCR with high-fidelity polymerase and sequenced the amplicons by GS-junior bench top system (Roche). Sequence data were analyzed with equipped software. "Coverage" indicates the total numbers of sequenced reads. (B) Frequencies of base substitutions in hyperedited *EGFP* genes. Base substitutions were classified to 6 groups and substituted base number of each group per 1,000 sequenced base pairs are show. (C) Dinucleotide contexts in genomic DNA editing. The rates of indicated dinucleotide sequence at the C to T transitions are shown. Deviations in the editing contexts do not reach statistical significance ($p < 0.01$) in a χ^2 test.

lymphoma cell lines consistent with prior work suggesting myeloid specificity[25,36]. *AID* transcripts were detected in 2 of 4 cell lines, which is consistent with previous studies[31,32,37]. We also examined expression of *A3B* in two lymph node samples of diffuse large B-cell lymphoma, and found that A3B is actually expressed (supplementary Fig. 3 online).

To investigate the correlation between *A3B* expression and frequency of somatic mutations, we next performed direct sequencing of *cMYC*, *PAX5*, and *A20* genes which are exemplary genes mutated frequently in B-cell lymphoma[33,38]. We compared mutation frequencies of these genes in SUDHL-6 and KIS-1, because the expression of *A3B* was the lowest in the former and the highest in the latter, while AID was not expressed in either cell line. DNA sequences between exon 1 and intron 1 of these three genes were analyzed (899 base pairs of *cMYC*, 1550 base pairs of *Pax5*, and 1088 base pairs of *A20*), since it have been reported that somatic mutations induced by cytidine deaminases were concentrated within 2 kb downstream from transcription initiation sites[33,34]. We found nine mutations within investigated sequences of *cMYC* and *PAX5* in KIS-1, but not in SUDHL-6, in which five of nine mutations detected were C/G to T/A transitions. On the other hand, no mutation was detected within sequenced region of *A20* in either cells (Fig 5b). To analyze ongoing mutations in the genome in individual cells, we next sequenced the same region of *cMYC* sub-cloned from KIS-1 and SUDHL-6, and found several more C to T mutations in KIS-1 cells, but not in SUDHL-6 cells (Supplementary Fig. S4 online). We next determined expression of these tumor-related genes by quantitative RT-PCR and found that the transcripts of *cMYC* and *PAX5* were highly expressed in both SUDHL6 and KIS1 cells as compared to PBL, whereas *A20* was less transcribed in these lymphoma cells. These results suggest that high expression of *A3B* resulted in accumulation of base alterations, especially C/G to T/A transitions, in actively transcribed tumor-related genes in lymphoma cells.

To ascertain more definitely that A3B can edit tumor-related genes in lymphoma cells, we introduced *A3B* into a lymphoma cell line and analyzed somatic mutations in *cMYC*. SUDHL-6 cells were transfected with expression vector for A3B WT, H66/253R, or mock by electroporation and total DNA was extracted after 7-day culture. With 3D-PCR analysis of *cMYC*, we obtained the amplicon from only A3B WT-expressing cells at the lower Td (Fig 6a). Clonal sequencing of amplicons at 85.9°C revealed 2 to 7 nucleotide substitutions per strand, and more than 80% of these mutations were C/G to T/A transitions, with a preference for 5′-GC dinucleotide sites (Fig 6b and c). We also sequenced the amplicons at 94.0°C of Td and

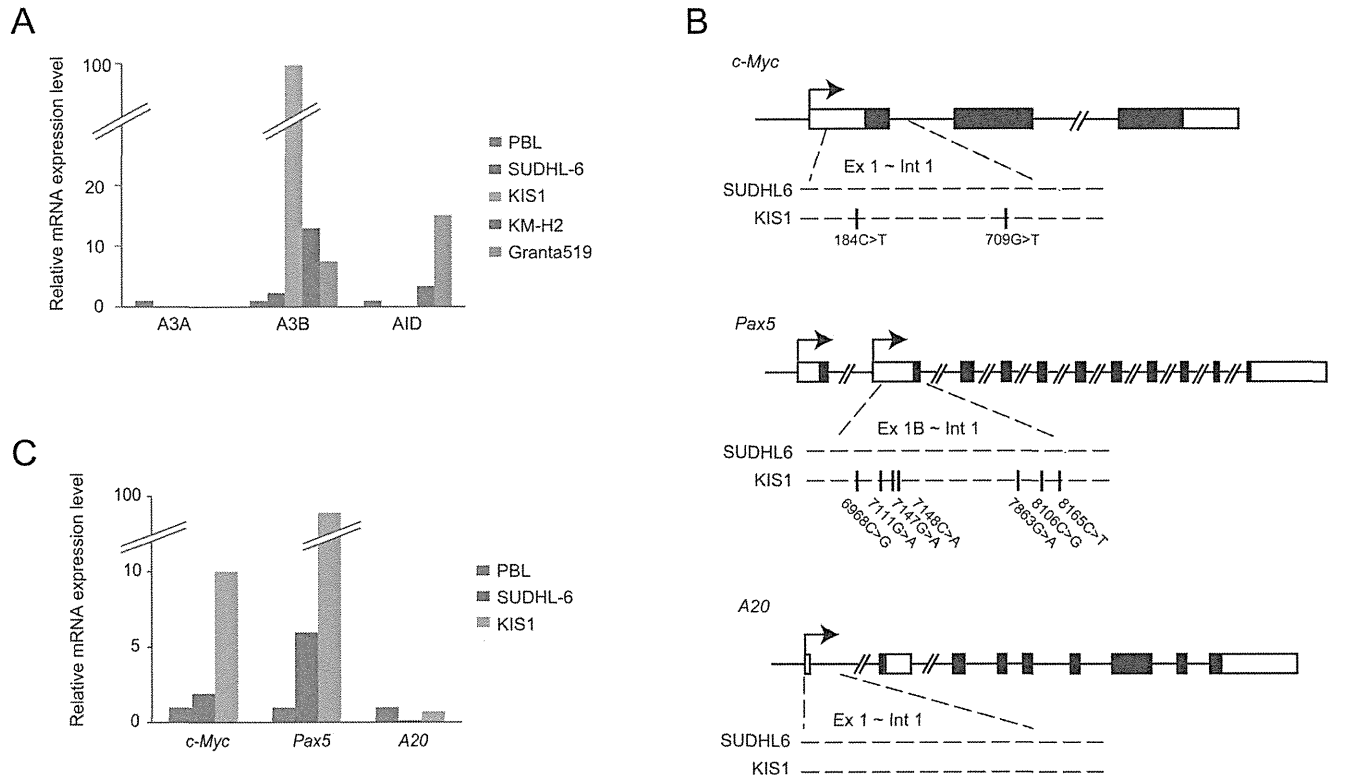

Figure 5 | Expression of *A3B* and somatic mutations in oncogenes in human lymphoma cell lines. (A) Quantitative RT-PCR for *A3A*, *A3B*, and *AID* in lymphoma cell lines. The levels of target cDNA were normalized to the endogenous hypoxanthine phosphoribosyl transferase 1 (*HPRT1*) and then compared to those in peripheral blood lymphocytes. (B) Mutational analyses of *C-myc*, *Pax5*, and *A20* in SUDH6 and KIS1 cells. We recovered total DNA from the cells and amplified the sequence between exon1 and intron1 of *C-myc*, *Pax5* and *A20* by PCR and performed direct sequencing of the amplicons. Locations of somatic mutations are shown below the loci with their positions. (C) The expression levels of transcripts of *C-myc*, *Pax5*, and *A20* in KIS1 and SUDHL6 cells. Quantitative RT-PCR was similarly performed with (a).

found A3B-induced C/G to T/A transitions without 5′-TC dinucleotide preference (supplementary Fig. 5 online). These data demonstrate that expression of A3B can induce somatic mutations into actively transcribed tumor-related genes in lymphoma cells.

Discussion

To date, most studies on A3 proteins have focused on their abilities as antiviral or antitransposon factors, whereas the capability of A3 proteins to induce mutations into genomic DNA in host cells has been scarcely verified. In contrast, many studies have elucidated that AID induces somatic mutations into not only Ig genes, but also tumor-related genes in human cells and that ubiquitous expression of AID in mice leads to cancers of various organs as well as lymphomas, with the accumulation of nucleotides alterations[9–13]. Thus, AID has been considered as the only DNA cytosine deaminase that can induce somatic mutations into human genome and has potential to cause cancers or hematologic malignancies.

Suspène *et al.* have recently reported that hyperediting of both mitochondrial and nuclear DNA was detected in human cells defective for UNG derived from hyper IgM syndrome patients and demonstrated that A3A-induced mutations in nuclear DNA are detectable under the condition of suppressing UNG in human cells[19]. In their report, deamination of nuclear DNA was not observed in cells expressing other A3 proteins or in cells expressing A3A without UNG suppression. Furthermore, Landry *et al.* have reported that expression of A3A together with UGI in mammalian cell lines resulted in breaking of DNA and activation of DNA damage response in a deaminase-dependent manner[18]. In these two reports, the effect on genomic integrity by A3A was dependent on the presence of UGI. Thus, there has been no direct evidence that A3 proteins induce mutations in genomic DNA in the cells with intact DNA repair systems.

In this study, we demonstrate that A3A and A3B as well as AID can induce C/G to T/A transitions into nuclear DNA without suppressing UNG by two different assays, 3D-PCR and deep sequencing. We assume that increased number of cytidine deamination catalyzed by highly expressed A3A or A3B exceeded the processivity of DNA repair enzymes such as UNG and resulted in leaving C/G to T/A transitions in nuclear DNA. Mutation frequencies were considerably lower compared to Suspène's report. However, Yoshikawa *et al.* reported that AID induced hypermutations into an actively transcribed gene in fibroblasts and that the mutation frequency was approximately 4 to 6 per 1000 base pairs[10], almost to the same extent as our results. Hence the frequency of mutations induced by cytidine deaminases into nuclear DNA is probably this extent or less in the cells with intact DNA repair systems.

We also find that *A3B* is highly expressed in several lymphoma cell lines and that the cells expressing high levels of *A3B* actually possesses somatic mutations, especially C/G to T/A transitions, in actively transcribed tumor-related genes. Furthermore, we reveal that introduction of *A3B* into lymphoma cells induces the accumulation of C/G to T/A transitions in *cMYC* gene. This is the first report that suggests the involvement of A3B in inducing somatic mutations of oncogenes in tumor cells. Together with the microarray database of A3B expression in miscellaneous cancer cell lines[14] (NextBio: http://www.nextbio.com), it is possible that A3B may induce somatic mutations into tumor related genes in various types of cancers.

Several questions remain open. First, it remains unclear what is preferred target sequences of A3 proteins in genomic DNA. Because

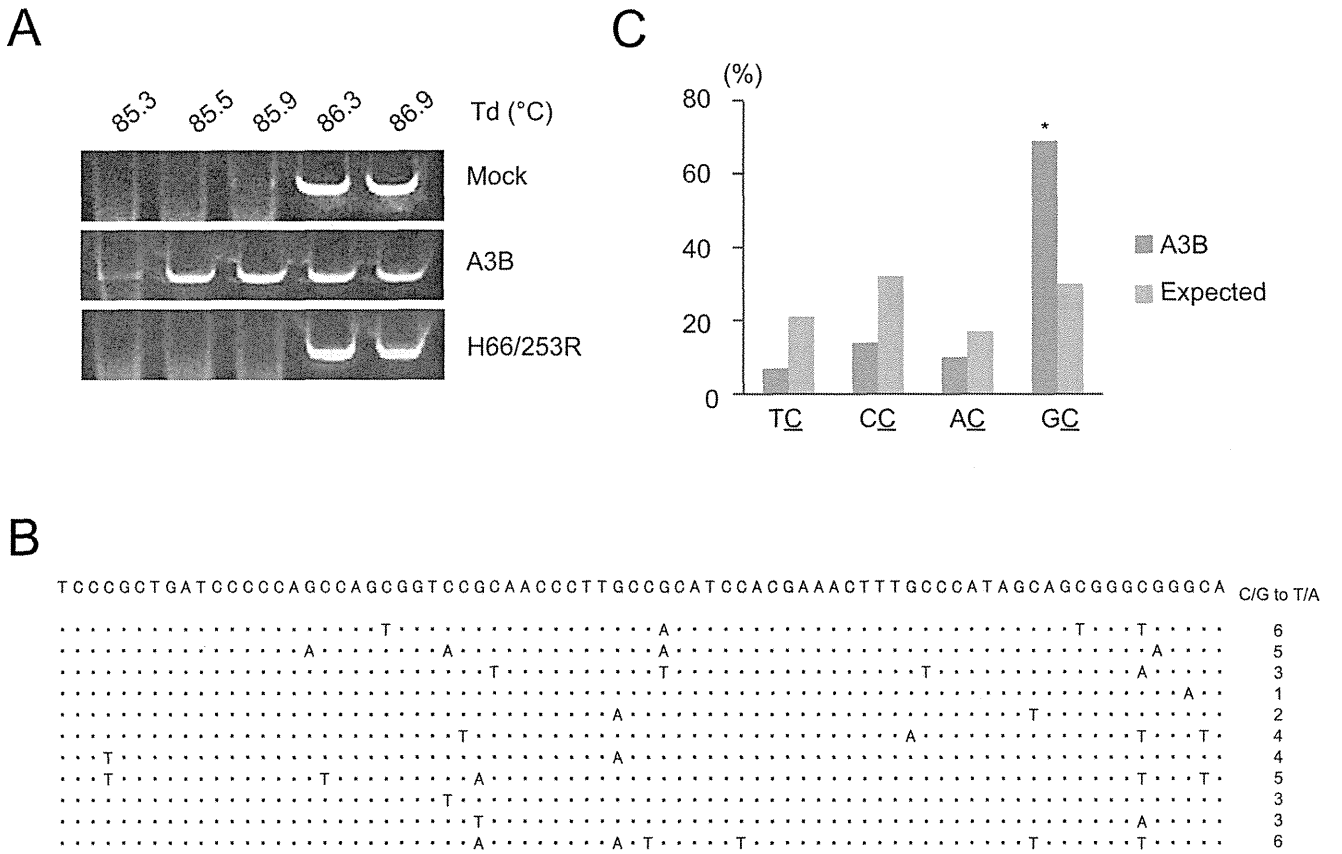

Figure 6 | A3B induced somatic mutations into *c-myc* gene in human lymphoma cells. (A) Agarose gel analyses of 3D-PCR products of *c-Myc* genes in SUDHL6. We transfected expression vector for A3B wild-type or H66/253R or empty vector and recovered total DNA 7 days after transfection. *C-myc* genes were amplified by 3D-PCR at the indicated denaturation temperatures (Td). (B) Clonal sequencing of amplicons from A3B-WT expressing SUDHL6 cells. We sequenced 11 clones (5104 base pairs in total). Seventy six bases from thymine 310 to adenine 385 in which mutations are concentrated among sequenced 464 base pairs are shown. The numbers of C/G to T/A substitutions in sequenced 464 base pair length are shown at the right end. (C) Dinucleotide contexts of somatic mutations in *c-Myc* gene by A3B. The rates of indicated dinucleotide sequence at the C to T transitions are shown. Asterisks indicate statistical significance in a χ^2 test ($p < 0.01$).

in several cancers such as breast cancer and melanoma, 5′-TC is the most prevalent target in C to T base substitutions, A3 is the most potential candidate to induce these mutations[25,28]. However, in our results, neither A3A nor A3B had a definite preference of editing site in nuclear DNA editing, whereas a preference for 5′-TC dinucleotide was observed in foreign DNA editing as previously reported. It is possible that A3A and A3B have no distinct favorite context in nuclear DNA editing, unlike viral and bacterial DNA editing, because human genomic DNA is more profoundly protected in transcription than viral or bacterial DNA and is under survey of DNA repair systems. However, Suspene *et al.* reported that target contexts of cytidine deamination in A3A+UGI-expressing cells were 5′-TC and 5′-CC dinucleotides, which were identical to the contexts of viral or bacterial DNA editing[19]. We assume that this discrepancy might be attributable to cell types or expression levels in cells. Hence, further analyses should be required to clarify the favorite target contexts of A3 proteins in nuclear DNA editing. The second question is how transcriptional control and post-translational modification of A3 proteins regulate A3 activity. Because the molecules that possess a capability of editing nuclear DNA threaten cell homeostasis, expression and activity of A3A and A3B must be strictly controlled. AID is known to be regulated at multiple steps[39], for example, transcriptional regulation[40–42], post-transcriptional regulation by micro-RNA[43,44], regulation of intracellular localization[45,46], and phosphorylation by PKA[47,48]. In contrast to AID, little is known about how A3 proteins are regulated. It has been reported that A3A is abundantly expressed in CD14+ monocytes and upregulated by interferon-α stimulation[25,49,50]. Meanwhile, it is not clear where A3B is expressed normally[25,42,49,50] and how it is regulated. As for post-translational modification, we previously reported that PKA-mediated phosphorylation of A3G regulates the interaction between A3G and HIV Vif[51]. To better understand the physiological roles of A3 proteins, it is important to elucidate how their expression and activity are regulated. The last question is whether A3 proteins can serve as an "initiator" of tumorigenesis. Our results suggest A3B indeed induces somatic mutations into genomic DNA in various human tumor cells, however, it is unclear whether A3B proteins impair genomic DNA from the early stage of oncogenesis. To address this question, hereafter, histopathological and genetic analyses of transgenic mouse constitutively expressing A3 proteins are necessary.

In conclusion, our findings provides the first evidence that A3A and A3B can induce C/G to T/G transitions into genomic DNA without suppressing DNA repair system. Our data also show that high expression of *A3B* is related to mutation frequencies of oncogenes in lymphoma cells. Our results suggest that *A3B* is an oncogene, like AID, which may have the capacity to evoke genomic instability through base substitutions in human cells. Further studies will be required to test whether endogenous A3B is capable of impairing genomic integrity as a DNA mutator and contributing to the development of human cancers and hematologic malignancies.

Methods

DNA constructs and cell lines. Plasmids containing coding sequence of human *A3A* and *A3B* were kindly provided by Dr. Kenzo Tokunaga[21]. Expression vectors for HA-tagged A3A, A3B and AID were generated by sub-cloning of coding sequences into pCAG-GS vector. A3B catalytic domain mutants (H66R, H253R, and H66/253R) were generated by KOD-plus mutagenesis Kit (Toyobo). Expression vector for Uracil-DNA glycosylase inhibitor, pEF-UGI was kindly provided by Dr. Ruben S Harris[25]. HEK293 and HEK293T cells were maintained with Dulbecco's modified Eagle's medium containing 10% of fetal bovine serum (FBS) and penicillin, streptomycin, and glutamine (PSG). All B-cell lymphoma cell lines were maintained with RPMI1640 containing 10% FBS and PSG. Retrovirus containing *EGFP* sequence was produced by co-transfection of pMLV gag-pol, VSV-G, and pDON-EGFP into HEK293T cells. HEK293/EGFP cells were generated by retroviral transduction of *EGFP* and selection of 1 mg/ml G418 for two months.

Immunoblotting. HEK293 cells were transfected with expression vector for A3A, A3B wild-type or mutant (H66R, H253R or H66/253R) or AID, and lysed with RIPA buffer (50 mM Tris-HCl pH7.5, 150 mM NaCl, 1 mM EDTA, 1% Triton-X, 0.1% SDS, 0.1% DOC) after 2-day culture. After centrifugation at 20,000 x g for 15 min, supernatant was mixed with sample buffer (Biorad), boiled for 5 minutes, resolved on 12% (w/v) polyacrylamide gel, transferred to PVDF membrane (Immobilon, Millipore), and analyzed by standard immunoblotting procedure with anti-HA monoclonal antibody (12CA5, Roche) or anti-β-actin monoclonal antibody (AC-15, Sigma).

3D-PCR and clonal sequencing. For foreign DNA editing assay, HEK293 cells were transfected with pEGFP-N3, pEF-UGI, and expression vector for A3A, A3B WT or mutant, or AID by using Fugene HD (Roche). After two-day culture, total DNA was extracted by using Quick Gene DNA whole blood kit (Fuji Film). First round PCR was performed with primers listed in Supplementary Table S2 using rTaq DNA polymerase (Takara), with the following reaction profile; 30 s at 94°C, 25cycles of 30 s at 94°C, 40 s at 62°C, and 90 s at 72°C followed by 10 min at 72°C. The amplicons were separated by electrophoresis on 1% (w/v) agarose gel, and extracted from the gel using Qiaquick Gel Extraction kit (Qiagen). We used 25 ng of first-round PCR products as template for nested PCR using Hotstar Hifidelity DNA polymerase (Qiagen), with the following reaction profile; 5 min at 95°C, 35 cycles of 15 s at 83–92°C, 60 s at 62°C, 80 s at 72°C, followed by 10 min at 72°C. The amplicons derived at 83.8°C were cloned into pT7-blue vector (Novagen). For nuclear DNA editing assay, HEK293/EGFP cells were transfected with expression vector for A3A, A3B WT or mutants, or AID using Fugene HD (Roche). Seven days after transfection, we extracted total DNA from these cells with the same method of foreign DNA editing assay. First round PCR was performed using Advantage HF2 polymerase kit (Clontech), with the following reaction profile;1 min at 94°C, 30 cycles of 30 s at 94°C followed by 2 min at 68°C, followed by 3 min at 68°C. We used 25 ng of first-round PCR products for nested PCR using Hotstar Hifidelity DNA polymerase (Qiagen) with the following reaction profile; 5 min at 95°C, 35 cycles of 15 s at 86–89°C, 60 s at 62°C, and 80 s at 72°C, followed by 10 min at 72°C. The amplicons derived at 86.5°C and 83.8°C were cloned into pT7-blue vector (Novagen). For *c-myc* gene editing assay in lymphoma cells, we transfected SUDHL6 cells with expression vectors for A3B WT or H66/253R by electroporation using Nucleofector (Amaxa) and extracted total DNA from the cells 7 days after transfection. First round PCR and gel extractions of amplicons were performed with the same methods of nuclear DNA editing assay. We used 25 ng of first-round PCR products for nested PCR using Hotstar Hifidelity DNA polymerase (Qiagen), with the following reaction profile; 5 min at 95°C, 35 cycles of 15 s at 85–88°C, 60 s at 62°C, 80 s at 72°C, followed by 10 min at 72°C. The amplicons derived at 85.3°C were cloned into pT7-blue vector (Novagen) and sequenced using 3130xl Genetic Analyzer (Applied Biosystems).

Deep sequencing. Total DNA was extracted from HEK293/EGFP transfected with expression vectors for A3A, A3B WT or H66/253R or AID 7 days after transfection. A portion of *EGFP* gene with 443 base pair length, from thymine 56 to cytosine 498, was amplified with the primers listed in Supplementary Table 2 using Advantage HF2 polymerase kit (Clontech), with the following reaction profile; 1 min at 94°C, 30 cycles of 30 s at 94°C followed by 2 min at 68°C, and followed by 3 min at 68°C. The amplicons were separated by electrophoresis on 1% (w/v) agarose gel, and extracted from the gel using Quiaquick Gel Extraction Kit (Qiagen). Purified amplicons were sequenced using GS junior bench top system (Roche) according to the manufacturer's protocol and analyzed with equipped software, GS Amplicon Variant Analyzer.

Lymphoma cell lines and patient samples. Four B-cell lymphoma cell lines (SUDHL6, KIS1, KM-H2, and Granta519) were cultured in RPMI1640 containing 10% of fetal bovine serum (FBS) and penicillin, streptomycin, and glutamine (PSG). We extracted total DNA from these cells by using Quick Gene DNA whole blood kit (Fuji Film) and total RNA by using mir Vana miRNA isolation kit (Ambion). Tumor biopsy specimens prior to treatment were obtained from two patients with diffuse large B-cell lymphoma. The study was approved by the Kyoto University Institutional Review Board and written informed consent was obtained from each patient. Total RNA were extracted similarly to lymphoma cell lines. Naïve B-cells were isolated from healthy donor's peripheral blood by using MACS® naive B cell isolation kit (Miltenyi Biotec).

Quantitative RT-PCR. Complementary DNA was synthesized from 200 ng of total RNA using Revertra Ace qPCR RT Master Mix (Toyobo). Real-time PCR were performed with Thunderbird SYBR qPCR Mix (Toyobo) according to manufacturer's protocol. Target cDNAs were normalized to the endogenous expression level of the house keeping reference gene for hypoxanthine-guanine phosphoribosyl transferase 1 (*HPRT1*) or glyceraldehyde 3-phosphate dehydrogenase (*GAPDH*). All primers for real-time PCR are listed in Supplementary Table 2.

Sequencing of oncogenes from lymphoma cell lines. We amplified portions of *C-myc*, *Pax5*, and *A20* from with the primers listed in Supplementary Table 2 using Advantage HF2 polymerase kit (Clontech), with the following reaction profile; 1 min at 94°C, 30 cycles of 30 s at 94°C followed by 4 min at 68°C, and followed by 3 min at 68°C. The amplicons were separated by electrophoresis on 1% (w/v) agarose gel, extracted from the gel using Qiaquick Gel Extraction kit (Qiagen), and sequenced using 3130xl Genetic Analyzer (Applied Biosystems). In *c-Myc* clonal sequencing, the amplicon was subcloned into pTA2-vector (TOYOBO) and subsequently sequenced.

1. Hahn, W. C. & Weinberg, R. A. Rules for making human tumor cells. *N Engl J Med* **347**, 1593–603 (2002).
2. Pleasance, E. D. *et al.* A comprehensive catalogue of somatic mutations from a human cancer genome. *Nature* **463**, 191–6 (2010).
3. Bronner, C. E. *et al.* Mutation in the DNA mismatch repair gene homologue hMLH1 is associated with hereditary non-polyposis colon cancer. *Nature* **368**, 258–61 (1994).
4. Greenman, C. *et al.* Patterns of somatic mutation in human cancer genomes. *Nature* **446**, 153–8 (2007).
5. Prickett, T. D. *et al.* Analysis of the tyrosine kinome in melanoma reveals recurrent mutations in ERBB4. *Nat Genet* **41**, 1127–32 (2009).
6. Macduff, D. A. & Harris, R. S. Directed DNA deamination by AID/APOBEC3 in immunity. *Curr Biol* **16**, R186–9 (2006).
7. Conticello, S. G. The AID/APOBEC family of nucleic acid mutators. *Genome Biol* **9**, 229 (2008).
8. Muramatsu, M. *et al.* Class switch recombination and hypermutation require activation-induced cytidine deaminase (AID), a potential RNA editing enzyme. *Cell* **102**, 553–63 (2000).
9. Matsumoto, Y. *et al.* Helicobacter pylori infection triggers aberrant expression of activation-induced cytidine deaminase in gastric epithelium. *Nat Med* **13**, 470–6 (2007).
10. Yoshikawa, K. *et al.* AID enzyme-induced hypermutation in an actively transcribed gene in fibroblasts. *Science* **296**, 2033–6 (2002).
11. Okazaki, I. M. *et al.* Constitutive expression of AID leads to tumorigenesis. *J Exp Med* **197**, 1173–81 (2003).
12. Pasqualucci, L. *et al.* AID is required for germinal center-derived lymphomagenesis. *Nat Genet* **40**, 108–12 (2008).
13. Endo, Y. *et al.* Activation-induced cytidine deaminase links between inflammation and the development of colitis-associated colorectal cancers. *Gastroenterology* **135**, 889–98, 898 e1-3 (2008).
14. Jarmuz, A. *et al.* An anthropoid-specific locus of orphan C to U RNA-editing enzymes on chromosome 22. *Genomics* **79**, 285–96 (2002).
15. Goila-Gaur, R. & Strebel, K. HIV-1 Vif, APOBEC, and intrinsic immunity. *Retrovirology* **5**, 51 (2008).
16. Mangeat, B. *et al.* Broad antiretroviral defence by human APOBEC3G through lethal editing of nascent reverse transcripts. *Nature* **424**, 99–103 (2003).
17. Bogerd, H. P. *et al.* Cellular inhibitors of long interspersed element 1 and Alu retrotransposition. *Proc Natl Acad Sci U S A* **103**, 8780–5 (2006).
18. Landry, S., Narvaiza, I., Linfesty, D. C. & Weitzman, M. D. APOBEC3A can activate the DNA damage response and cause cell-cycle arrest. *EMBO Rep* **12**, 444–50 (2011).
19. Suspène, R. *et al.* Somatic hypermutation of human mitochondrial and nuclear DNA by APOBEC3 cytidine deaminases, a pathway for DNA catabolism. *Proc Natl Acad Sci U S A* **108**, 4858–63 (2011).
20. Lackey, L. *et al.* APOBEC3B and AID have similar nuclear import mechanisms. *J Mol Biol* **419**, 301–14 (2012).
21. Kinomoto, M. *et al.* All APOBEC3 family proteins differentially inhibit LINE-1 retrotransposition. *Nucleic Acids Res* **35**, 2955–64 (2007).
22. Bogerd, H. P., Wiegand, H. L., Doehle, B. P. & Cullen, B. R. The intrinsic antiretroviral factor APOBEC3B contains two enzymatically active cytidine deaminase domains. *Virology* **364**, 486–93 (2007).
23. Suspène, R. *et al.* Extensive editing of both hepatitis B virus DNA strands by APOBEC3 cytidine deaminases in vitro and in vivo. *Proc Natl Acad Sci U S A* **102**, 8321–6 (2005).
24. Bonvin, M. & Greeve, J. Effects of point mutations in the cytidine deaminase domains of APOBEC3B on replication and hypermutation of hepatitis B virus in vitro. *J Gen Virol* **88**, 3270–4 (2007).
25. Stenglein, M. D., Burns, M. B., Li, M., Lengyel, J. & Harris, R. S. APOBEC3 proteins mediate the clearance of foreign DNA from human cells. *Nat Struct Mol Biol* **17**, 222–9 (2010).
26. Suspène, R., Henry, M., Guillot, S., Wain-Hobson, S. & Vartanian, J. P. Recovery of APOBEC3-edited human immunodeficiency virus G->A hypermutants by differential DNA denaturation PCR. *J Gen Virol* **86**, 125–9 (2005).

27. Vartanian, J. P. *et al.* Massive APOBEC3 editing of hepatitis B viral DNA in cirrhosis. *PLoS Pathog* **6**, e1000928 (2010).
28. Bishop, K. N. *et al.* Cytidine deamination of retroviral DNA by diverse APOBEC proteins. *Curr Biol* **14**, 1392–6 (2004).
29. Harris, R. S. *et al.* DNA deamination mediates innate immunity to retroviral infection. *Cell* **113**, 803–9 (2003).
30. Beale, R. C. *et al.* Comparison of the differential context-dependence of DNA deamination by APOBEC enzymes: correlation with mutation spectra in vivo. *J Mol Biol* **337**, 585–96 (2004).
31. Greeve, J. *et al.* Expression of activation-induced cytidine deaminase in human B-cell non-Hodgkin lymphomas. *Blood* **101**, 3574–80 (2003).
32. Deutsch, A. J. *et al.* MALT lymphoma and extranodal diffuse large B-cell lymphoma are targeted by aberrant somatic hypermutation. *Blood* **109**, 3500–4 (2007).
33. Pasqualucci, L. *et al.* Hypermutation of multiple proto-oncogenes in B-cell diffuse large-cell lymphomas. *Nature* **412**, 341–6 (2001).
34. Kotani, A. *et al.* A target selection of somatic hypermutations is regulated similarly between T and B cells upon activation-induced cytidine deaminase expression. *Proc Natl Acad Sci U S A* **102**, 4506–11 (2005).
35. Smit, L. A. *et al.* Expression of activation-induced cytidine deaminase is confined to B-cell non-Hodgkin's lymphomas of germinal-center phenotype. *Cancer Res* **63**, 3894–8 (2003).
36. Chen, H. *et al.* APOBEC3A is a potent inhibitor of adeno-associated virus and retrotransposons. *Curr Biol* **16**, 480–5 (2006).
37. Mottok, A., Hansmann, M. L. & Bräuninger, A. Activation induced cytidine deaminase expression in lymphocyte predominant Hodgkin lymphoma. *J Clin Pathol* **58**, 1002–4 (2005).
38. Kato, M. *et al.* Frequent inactivation of A20 in B-cell lymphomas. *Nature* **459**, 712–6 (2009).
39. Delker, R. K., Fugmann, S. D. & Papavasiliou, F. N. A coming-of-age story: activation-induced cytidine deaminase turns 10. *Nat Immunol* **10**, 1147–53 (2009).
40. Crouch, E. E. *et al.* Regulation of AID expression in the immune response. *J Exp Med* **204**, 1145–56 (2007).
41. Gonda, H. *et al.* The balance between Pax5 and Id2 activities is the key to AID gene expression. *J Exp Med* **198**, 1427–37 (2003).
42. Pauklin, S., Sernández, I. V., Bachmann, G., Ramiro, A. R. & Petersen-Mahrt, S. K. Estrogen directly activates AID transcription and function. *J Exp Med* **206**, 99–111 (2009).
43. Teng, G. *et al.* MicroRNA-155 is a negative regulator of activation-induced cytidine deaminase. *Immunity* **28**, 621–9 (2008).
44. de Yébenes, V. G. *et al.* miR-181b negatively regulates activation-induced cytidine deaminase in B cells. *J Exp Med* **205**, 2199–206 (2008).
45. Ito, S. *et al.* Activation-induced cytidine deaminase shuttles between nucleus and cytoplasm like apolipoprotein B mRNA editing catalytic polypeptide 1. *Proc Natl Acad Sci U S A* **101**, 1975–80 (2004).
46. Patenaude, A. M. *et al.* Active nuclear import and cytoplasmic retention of activation-induced deaminase. *Nat Struct Mol Biol* **16**, 517–27 (2009).
47. Basu, U. *et al.* The AID antibody diversification enzyme is regulated by protein kinase A phosphorylation. *Nature* **438**, 508–11 (2005).
48. McBride, K. M. *et al.* Regulation of class switch recombination and somatic mutation by AID phosphorylation. *J Exp Med* **205**, 2585–94 (2008).
49. Koning, F. A. *et al.* Defining APOBEC3 expression patterns in human tissues and hematopoietic cell subsets. *J Virol* **83**, 9474–85 (2009).
50. Berger, G. *et al.* APOBEC3A is a specific inhibitor of the early phases of HIV-1 infection in myeloid cells. *PLoS Pathog* **7**, e1002221 (2011).
51. Shirakawa, K. *et al.* Phosphorylation of APOBEC3G by protein kinase A regulates its interaction with HIV-1 Vif. *Nat Struct Mol Biol* **15**, 1184–91 (2008).

Acknowledgments

We thank R. Harris for thoughtful feedback and for UGI vector, and K. Tokunaga for A3A and A3B vectors.

Author contributions

M.S. performed most of the experiments, analyzed the data and wrote the manuscript; I.K., M.M., T.S. and K.T. performed sequencing of lymphoma cell lines; K.S. and N.K. wrote the manuscript; M.K. established q-PCR; A.T.K. designed the experiments and wrote the manuscript.

Additional information

Supplementary information accompanies this paper at http://www.nature.com/scientificreports

Competing interest statements: The authors declare no competing financial interests.

How to cite this article: Shinohara, M. *et al.* APOBEC3B can impair genomic stability by inducing base substitutions in genomic DNA in human cells. *Sci. Rep.* 2, 806; DOI:10.1038/srep00806 (2012).

Molecular Cell
Article

Poly-ADP Ribosylation of Miki by tankyrase-1 Promotes Centrosome Maturation

Yuko Ozaki,[1,7] Hirotaka Matsui,[1,7] Hiroya Asou,[1] Akiko Nagamachi,[1] Daisuke Aki,[1] Hiroaki Honda,[2] Shin'ichiro Yasunaga,[3] Yoshihiro Takihara,[3] Tadashi Yamamoto,[4,5] Shunsuke Izumi,[6] Miho Ohsugi,[4] and Toshiya Inaba[1,*]
[1]Department of Molecular Oncology and Leukemia Program Project
[2]Department of Disease Model
[3]Department of Stem Cell Biology
Research Institute for Radiation Biology and Medicine, Hiroshima University, Hiroshima 734-8553, Japan
[4]Division of Oncology, Institute of Medical Science, University of Tokyo, Tokyo 108-8639, Japan
[5]Cell Signal Unit, Okinawa Institute of Science and Technology, Onna-son, Okinawa 904-0412, Japan
[6]Graduate School of Science, Hiroshima University, Higashihiroshima 739-8511, Japan
[7]These authors contributed equally to this work
*Correspondence: tinaba@hiroshima-u.ac.jp
http://dx.doi.org/10.1016/j.molcel.2012.06.033

SUMMARY

During prometaphase, dense microtubule nucleation sites at centrosomes form robust spindles that align chromosomes promptly. Failure of centrosome maturation leaves chromosomes scattered, as seen routinely in cancer cells, including myelodysplastic syndrome (MDS). We previously reported that the *Miki* (*LOC253012*) gene is frequently deleted in MDS patients, and that low levels of Miki are associated with abnormal mitosis. Here we demonstrate that Miki localizes to the Golgi apparatus and is poly(ADP-ribosyl)ated by tankyrase-1 during late G2 and prophase. PARsylated Miki then translocates to mitotic centrosomes and anchors CG-NAP, a large scaffold protein of the γ-tubulin ring complex. Due to impairment of microtubule aster formation, cells in which tankyrase-1, Miki, or CG-NAP expression is downregulated all show prometaphase disturbances, including scattered and lagging chromosomes. Our data suggest that PARsylation of Miki by tankyrase-1 is a key initial event promoting prometaphase.

INTRODUCTION

Prometaphase is the phase of mitosis when robust mitotic spindles move chromosomes toward the center of the cell and align them on the metaphase plate. If the mechanism(s) promoting progression of prometaphase is impaired, chromosomes are left scattered for an extended period. One example of this is the downregulation of tankyrase-1, one of 18 mammalian poly(ADP-ribose) polymerases (PARPs), which results in severe mitotic defects in prometaphase such as preanaphase arrest, chromosome scattering, and "pseudometaphase" (several lagging chromosomes juxtaposed to, or even behind, spindle poles during metaphase chromosome alignment) (Chang et al., 2005a, 2005b). More recently, downregulation of ch-TOG/XMAP215, a microtubule-processing polymerase that "surfs" on growing microtubule plus ends, was reported to delay prometaphase and to induce pseudometaphase phenotypes (Brouhard et al., 2008; Gergely et al., 2003).

Chromosome scattering and pseudometaphase phenotypes are seen routinely in certain cancer cells, but the molecular mechanisms underlying these abnormalities are largely unknown (Nigg, 2002). Myelodysplastic syndrome (MDS), a common hematopoietic disease previously termed "preleukemia," is one such disease showing abnormal mitoses including so-called colchicine-mitosis (chaotic chromosome scattering similar to colchicine-treated cells) or lagging chromosomes, and subsequent abnormal nuclear morphologies, such as multinucleated cells with micronuclei.

We recently identified a common microdeletion cluster in the long arm of chromosome 7 (Asou et al., 2009), which is a region well known to be frequently deleted in MDS cells (Mauritzson et al., 2002). This microdeletion cluster contains three contiguous genes, *Samd9*, *Samd9L*, and *LOC253012*, each encoding a different product with few known functional motifs. Orthologs of these three genes are found only in vertebrate genomes, and not in invertebrates, plants, yeast, or prokaryotes.

The *Samd9* and *Samd9L* genes result from duplication of a common ancestral gene. Downregulation of Samd9 has also been reported in aggressive fibromatosis (Li et al., 2007). In addition, we recently observed that *Samd9L*-deficient mice develop myeloid malignancies at high frequency (our unpublished data), suggesting that Samd9 and Samd9L are tumor suppressors.

The LOC253012 gene product that we named Miki (mitotic kinetics regulator) translocates from the Golgi apparatus to mitotic centrosomes/spindles in late G2/M phase. Downregulation of this gene in HeLa cells induces prometaphase delay or arrest, with deeply disturbed chromosome alignment including chromosome scattering; pseudometaphase; and consequent bi-, tri-, or multinucleated cells with micronuclei. Intriguingly, Miki expression levels in MDS cells are associated with the abnormal mitosis and nuclear morphology that characterize MDS (Asou et al., 2009).

Here we focus on the function of Miki in mitosis. We demonstrate that Miki is a substrate for tankyrase-1. In late G2 to prophase, tankyrase-1 and PARsylated Miki translocate from the Golgi apparatus to mitotic centrosomes and play critical roles in the formation of robust microtubules for prompt movement of chromosomes.

RESULTS

Localization of Miki to Mitotic Spindles/Centrosomes

Miki (LOC253012 gene product) contains three domains suggestive of a cell surface protein, namely an N-terminal putative signal peptide, a central region with homology to immunoglobulin superfamily cell adhesion molecules (IgCAM), and an extremely hydrophobic transmembrane (TM) domain-like region (Figure 1A).

Unexpectedly, immunostaining of HeLa cells using antibodies against the C terminus of Miki showed an intense signal in the perinuclear region that colocalized with *trans*-Golgi markers such as p230 during interphase (Figure 1B, upper panels), as we previously reported (Asou et al., 2009). Localization of Miki in the Golgi apparatus was confirmed by FLAG immunostaining of HeLa cells expressing C-terminal FLAG-tagged full-length Miki (Miki-FLAG) protein transfected by the MSCV pantropic retrovirus (Figure 1C, middle panels). In contrast, only a small amount of a Miki(ΔN)-FLAG mutant lacking 30 N-terminal amino acids accumulated in the Golgi body (lower panels).

Although Miki does not appear to accumulate in centrosomes during interphase (Figure 1B, lower panels, insets), Miki immunostaining localizes to centrosomes and spindles during prophase, prometaphase, and metaphase of mitosis, and to midbodies at telophase (Figure 1D). Miki-FLAG protein was also detected in mitotic spindles and centrosomes by FLAG antibody (Figure 1E). However, the lack of putative signal peptide greatly reduced the accumulation of Miki(ΔN)-FLAG protein at spindle poles.

Because the antibodies we raised to detect endogenous Miki expression by immunoblotting did not unequivocally detect Miki protein in whole-cell extracts (Asou et al., 2009), we attempted to detect it in extracts from isolated mitotic spindles/centrosomes using a published method (Sillje and Nigg, 2006). Immunoblotting of lysates extracted from isolated mitotic spindles/centrosomes (Figure 1F) showed a band of ~50 kDa, corresponding to the predicted molecular weight of Miki (50.1 kDa), as well as an additional intense large band of ~125 kDa (Figure 1G), which comigrates with a G2/M phase-dominant band detected in whole-cell extracts (see Figure S1 online).

A large protein of ~125 kDa was also detected in immunoprecipitated products of HeLa cells using Miki antibody (Figure 1H, lane 5, arrowhead). We used MALDI-TOF spectroscopy to verify the identity of the immunoprecipitated p125 protein, and peptide mass fingerprinting to determine the molecular weights of the nine peaks resulting from the 125 kDa band. These were found to match the specific masses of Miki tryptic peptide fragments (Figure 1I). Mass spectrometric sequencing of these peaks confirmed that they matched Miki peptide sequences. These data suggest that $p125^{Miki}$ is present in mitotic centrosomes/spindles.

Prometaphase Arrest Resulting in Apoptosis Caused by Miki Downregulation

We previously selected two short-interfering (si) RNAs (siRNA#79 and siRNA#80; Asou et al., 2009) that effectively downregulate Miki expression in HeLa cells (Figure 2A). Upon treatment of HeLa cells with siRNA#80 (100 nM) for 48 hr, the number of floating mitotic cells significantly ($p < 0.01$) increased from 6.1% (control siRNA-treated cells) to 24.3% (siRNA#80-treated cells), suggesting that Miki downregulation disturbs mitosis. Indeed, in mitotic cells treated with siRNA#80 and stained with Hoechst 33342, we frequently observed more than three lagging chromosomes juxtaposed to, or even situated behind, spindle poles during metaphase chromosome alignment (Figure 2B, panel 1, arrows). This is similar to the "pseudometaphase" condition defined by others (Weaver et al., 2003), which is distinct from normal late prometaphase, when less than two (typically only one) lagging chromosomes are located near aligned chromosomes (panel 2, arrow). Mixed mitotic cell (MMC) culture that allows comparison of immunofluorescence signals from mitotic cells treated with different siRNAs (see the Experimental Procedures) revealed that cells with pseudometaphase phenotypes (panels 3 and 4, right-hand cell) showed markedly reduced Miki immunofluorescence signals compared with cells at metaphase (left-hand cell).

Pseudometaphase was observed in 6.7%–18.5% of mitotic cells treated with different concentrations of either siRNA#79 or siRNA#80 (Figure 2C). In contrast, cells treated with control siRNA (200 nM) rarely (<1%) showed pseudometaphase. In addition, a significant increase in telophase cells was also observed in cells treated with siRNA#79 (200 nM) and siRNA#80 (50 nM).

We established U2OS cells constitutively expressing a histone H2B-GFP fusion protein (Ozaki et al., 2011; Shi and King, 2005) and acquired time-lapse images following transfection with siRNAs (efficiency typically 80%). When cells were treated with control siRNA (100 nM) for 36 hr, ~90% of prophase U2OS cells entered anaphase within 45 min (Figure 2D). Early prometaphase in these cells is very short (Movie S1), and within 10 min, most chromosomes were aligned, with few lagging chromosomes near the metaphase plate. In contrast, treatment of cells with siRNA#80 (100 nM) for 36 hr resulted in only 24% of prophase cells entering anaphase within 45 min, and 28% of prophasic cells with prolonged prometaphase (typically around 90 min) (Figure 2D). The rest of the prophasic cells (48%) did not enter anaphase during the 12 hr observation period (Movie S2). In these prometaphase cells, chromosomes appeared to be scattered widely and randomly. Thereafter, the majority of chromosomes lined up transiently at the metaphase plate, but there were a few that did not. Occasionally, scattered chromosomes appeared to rotate synchronously around the cell center, suggesting highly motile spindle poles. Time-lapse observations of U2OS cells expressing a GFP-α-tubulin fusion protein confirmed the rotation of the spindles (Movie S3).

During a 12 hr observation period 36 hr after transfection of siRNA#80, 36% of the transfected cells underwent cell death (Figure 2D, Movie S4). Consistent with this, cells treated with siRNA#80 showed a significant increase in the numbers of annexin V- or TUNEL-positive cells, as well as cells with high

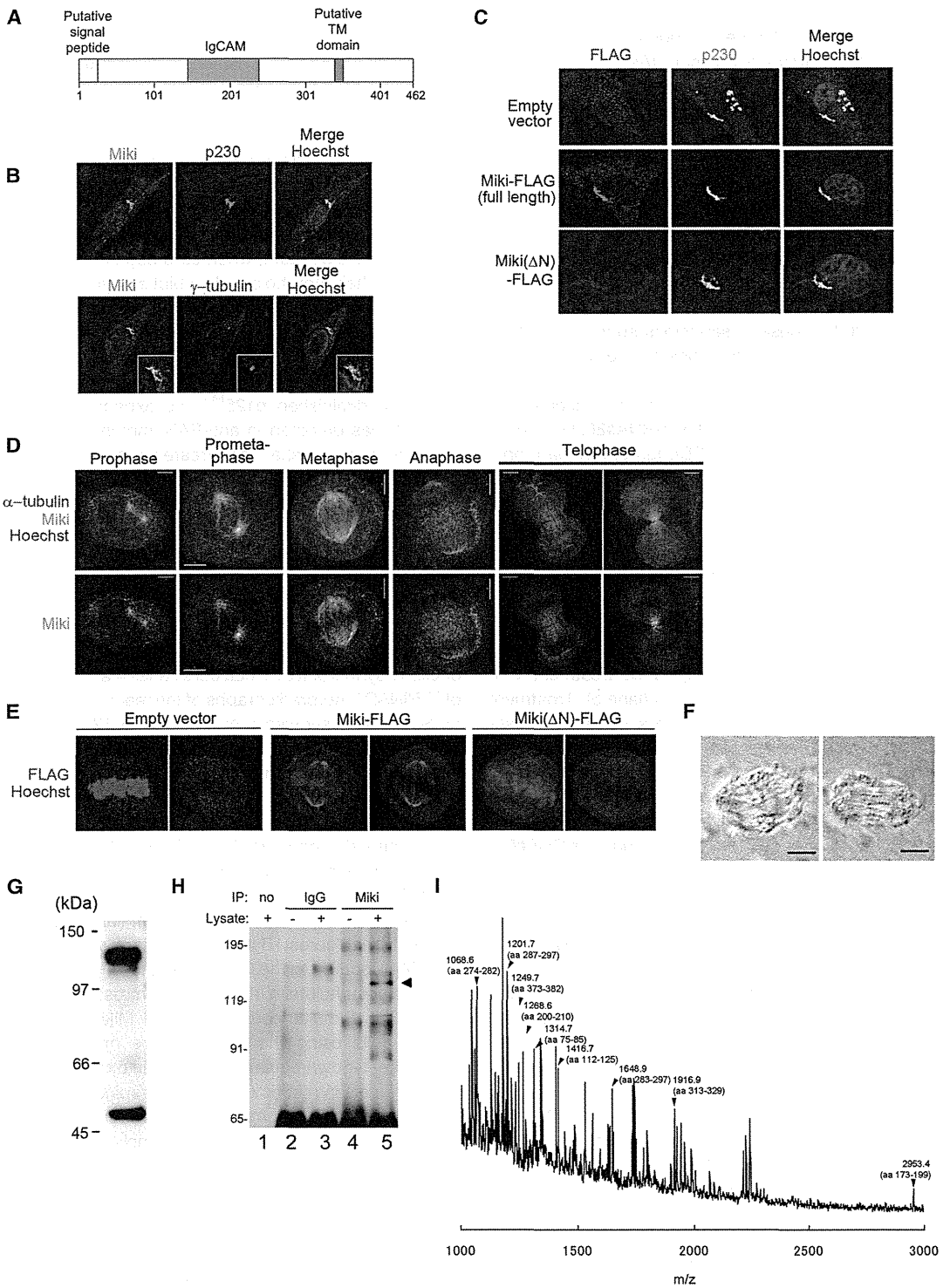

Figure 1. Detection of Miki

(A) Putative functional domains of Miki protein.

(B–E) Immunostaining of HeLa cells in interphase (B and C) or mitosis (D and E) with antibodies indicated above (B and C) or at left (D and E). Nuclear DNA was stained with Hoechst 33342. Insets show enlargements of a centrosomal area (B).

(F) Differential interference contrast (DIC) light microscopy image of isolated mitotic spindles. Scale bar, 5 μm.

caspase-3 activity relative to control untreated cells or cells treated with Miki siRNA#81 (Figure 2E, Figure S2), which does not interfere with Miki mRNA expression (Asou et al., 2009). These data demonstrate that Miki downregulation results in prometaphase delay or arrest, followed by subsequent initiation of apoptosis.

Another subset of cells treated with siRNA#80 showed chromosome decondensation and exit from mitosis in the absence of chromosome segregation (Figure 2F, arrow 1). This resulted in the accumulation of cells containing multiple nuclei of various sizes (arrow 2; arrow 3 shows a normal interphasic nucleus). Together with the overall increase in binucleated cells following Miki downregulation by constitutive expression of short-hairpin RNA (Asou et al., 2009), these observations suggest that Miki downregulation induces abnormal nuclear morphology and long-term chromosomal instability.

To test whether exogenously expressed Miki rescues the pseudometaphase phenotype induced by siRNA#80, HeLa cells were infected with either MSCV/ires-CD8 (an empty pantropic retrovirus) or MSCV-Miki^{MT80}/ires-CD8 (Miki^{MT80} contains the full-length Miki cDNA harboring silent mutations in the target sequence of siRNA#80). CD8-positive cells were then sorted with magnetic beads. Immunoblotting revealed that treatment of cells expressing Miki^{MT80} with siRNA#79 (with a target sequence conserved in Miki^{MT80}) reduced p125^{Miki} and *n*-glycosylated exogenously expressed Miki (Asou et al., 2009) to less than 20% of the amount found in untreated cells or cells treated with control siRNA (Figure 2G, lane 4), while treatment with siRNA#80 decreased p125^{Miki} by only 25% (lane 5). Treatment of control cells (infected with empty retrovirus) or cells expressing Miki^{MT80} with control siRNA did not induce pseudometaphase (Figure 2H). Treatment with siRNA#79 induced a significant increase of cells in pseudometaphase in both controls and cells expressing Miki^{MT80}. Similar changes were also observed in siRNA#80-treated control cells, but not in siRNA#80-treated cells expressing Miki^{MT80}, indicating that exogenous Miki aligns chromosomes promptly.

PARsylation of Miki by tankyrase-1 during Late G2/M Phase

Recent studies indicate that poly(ADP-ribose) (PAR) is enriched in vertebrate mitotic spindles and is required for spindle assembly and function (Chang et al., 2004). PAR perturbation by PAR glycohydrolase (PARG) or anti-PAR antibody results in rapid loss of spindle structure in *Xenopus* eggs. Indeed, in HeLa cells, immunoblotting of isolated mitotic spindles (Figure 1F) with PAR antibody showed marked accumulation of PAR (Figure 3A, lane 2) relative to the cytosolic fraction (lane 1).

More recently, downregulation of tankyrase-1 has been reported to result in severe mitotic defects in prometaphase such as preanaphase arrest, chromosome scattering, and pseudometaphase (Chang et al., 2005a, 2005b). Indeed, tankyrase-1-downregulation (Figure 3B, lane 2) using siRNA (Dynek and Smith, 2004) caused a significant increase of cells in pseudometaphase (Figure 2C), which was reversed by the forced expression of a tankyrase-1 cDNA that contains silent mutations in the target sequence of the siRNA (Figure 3B, lane 3; Figure S4).

These data raised the possibility that p125^{Miki} is Miki that has been PARsylated by tankyrase-1. PAR-antibody immunoblots of anti-PAR immunoprecipitates (of whole-cell extracts) revealed an accumulation of PARsylated polypeptides 9 hr after thymidine release (Figure 3C, top), when cells began to enter M phase as judged by their morphology. In a blot applying the same precipitation products, Miki antibody detected an ~125 kDa band (bottom). Conversely, PAR antibody immunoblots of anti-Miki immunoprecipitates revealed p125^{Miki} in G2/M, but not in G1 cells (Figure 3D, lanes 1 and 2). Downregulation of Miki by siRNA#80 diminished p125^{Miki}, as expected (lane 4). Finally, p125^{Miki} was detected in anti-PAR immunoprecipitates of G2/M-synchronized HeLa cells treated with control siRNA (Figure 3E, lane 1), as expected from the results shown in Figure 3C. However, it was not seen in cells treated with tankyrase-1 siRNA or Miki siRNA#80 (lanes 2 and 3). These data indicate that for a short period during late G2/M phase, p125^{Miki} is in fact PARsylated Miki.

PARsylation of Miki by tankyrase-1 was then tested directly by incubating in vitro-synthesized and purified Miki protein (Figure 3F, lane 2) with tankyrase-1 immunoprecipitated from G1- or G2/M-synchronized HeLa cells (lanes 4 and 5) in the presence of [^{32}P]NAD$^+$. Autoradiographs of the reaction products resolved by SDS-PAGE showed a smear around 120 kDa representing tankyrase-1 PARsylated Miki (lanes 10 and 13). This was no longer seen on treatment with 3-aminobenzamide, a PARP inhibitor (lanes 11 and 14). Intriguingly, tankyrase-1 from G2/M cells PARsylated Miki 4.2-fold more efficiently than that from G1 phase cells (compare lane 10 with 13). This was probably because tankyrase-1 is activated by phosphorylation during the G2/M phase via glycogen synthase kinase (GSK)-3 (Yeh et al., 2006), shown by a migration shift (lane 5, arrowhead).

Both Miki (Figures 1B and 1C) and tankyrase-1 (Chi and Lodish, 2000) localize to the Golgi apparatus (Figure 3G) but did not seem to accumulate in interphasic centrosomes (Figure 1B and Figure 3H). Simultaneous staining of Miki and tankyrase-1 in mitotic cells using the MMC culture method revealed that tankyrase-1-downregulation resulted in diminished Miki fluorescence signals in mitotic centrosomes/spindles (Figure 3I, panel 5, right-hand cell). In contrast, Miki downregulation did not affect tankyrase-1 levels in centrosomes (panel 4, right-hand cell), suggesting that Miki (but not tankyrase-1) in mitotic centrosomes/spindles plays a role in the promotion of prometaphase.

The significance of PARsylation was assessed using the Miki(ΔN) mutant containing silent mutations in the target sequence of siRNA#80. Like the full-length Miki, in vitro-translated

(G) Miki antibody immunoblots of isolated mitotic spindles and centrosomes.
(H) Lysates from HeLa cells (lanes 1, 3, and 5) or lysis buffer alone (lanes 2 and 4) were immunoprecipitated with no antibody (lane 1), control rabbit IgG (lanes 2 and 3), or Miki antibody (lanes 4 and 5). The resulting immunoprecipitates were blotted and reacted with Miki antibody for immunodetection.
(I) A representative result of peptide mass fingerprinting from MALDI-TOF analysis. The molecular weight of each peak and the corresponding amino acid residues of Miki confirmed by MAS sequencing analysis are shown.

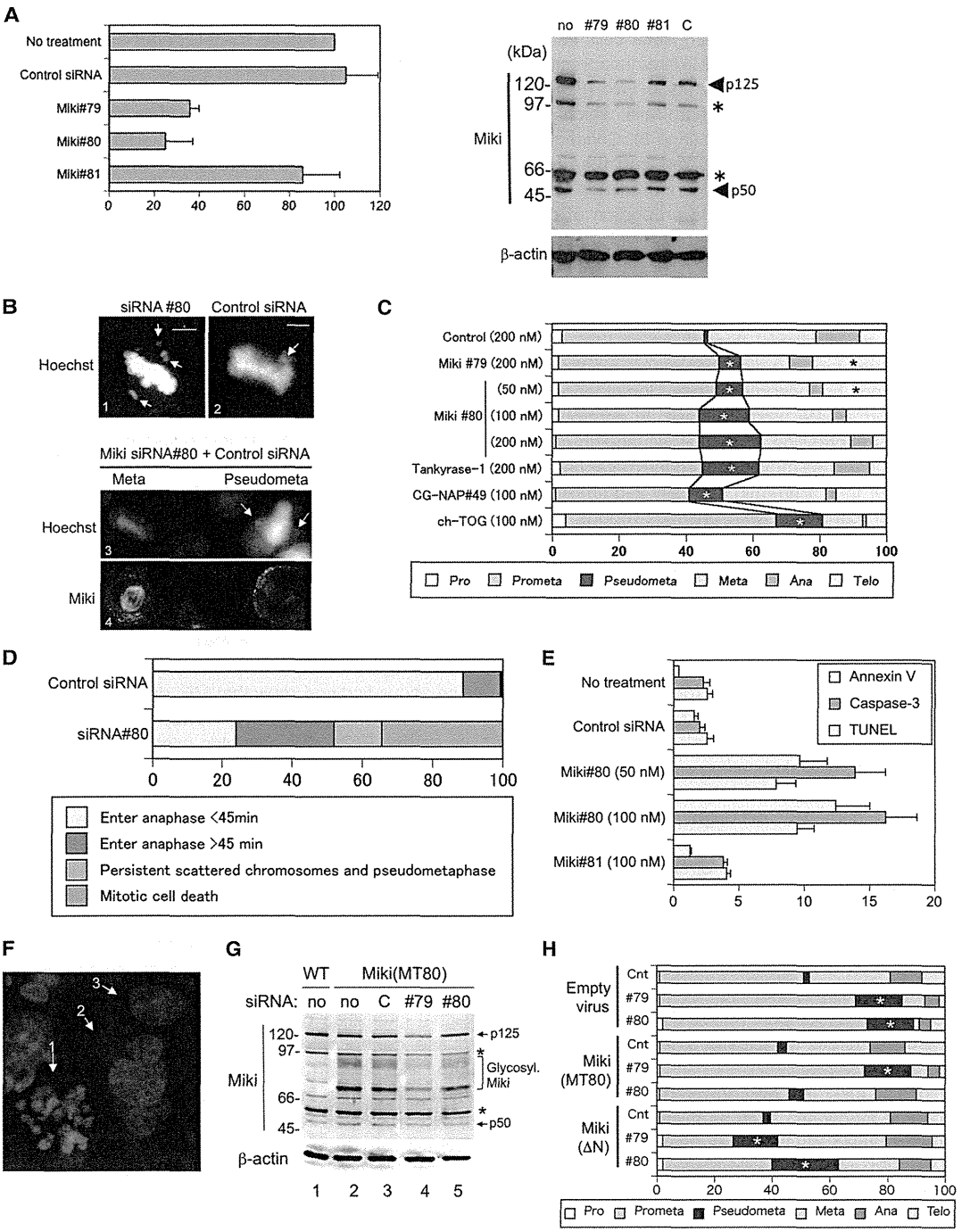

Figure 2. Downregulation of Miki Perturbs Prometaphase

(A) Miki mRNA measured using qRT-PCR and expressed as percent signal relative to an untreated control (left) and Miki or β-actin antibody immunoblots (right) of HeLa cells treated with the indicated siRNA for 24 hr. The mean and SD for four independent experiments are shown (left).

(B) Shown is staining with Hoechst 33342 (panels 1–3) and Miki antibody (panel 4) of mitotic HeLa cells treated with siRNA#80 (panel 1), control siRNA (panel 2), or MMC culture (panels 3 and 4) for 48 hr (100 nM, each).

(C and H) HeLa cells (C) or cells infected either with the MSCV empty retrovirus, virus containing Miki^{MT80}, or Miki(ΔN) cDNA (H) were treated with the siRNA indicated at left for 48 hr (100 nM, except otherwise indicated). Percentages of 200 cells in each mitotic phase or undergoing abnormal mitosis were calculated from observations of Hoechst 33342-stained nuclei. Asterisks indicate a significant increase relative to the control.